Toggweiler

Reprinted From *The Carbon Cycle and Atmospheric CO_2: Natural Variations Archean to Present*
Geophysical Monograph 32

GLACIAL TO INTERGLACIAL CHANGES IN ATMOSPHERIC CARBON DIOXIDE: THE CRITICAL ROLE OF OCEAN SURFACE WATER IN HIGH LATITUDES

J.R. Toggweiler and J.L. Sarmiento

Geophysical Fluid Dynamics Program, Princeton University
Princeton, New Jersey 08542

Abstract. Recent measurements of the CO_2 content of air bubbles trapped in glacial ice have shown that the partial pressure of atmospheric CO_2 during the last ice age was about 70 ppm lower than during the interglacial. Isotopic measurements on surface- and bottom-dwelling forams living during the ice age have shown that the $^{13}C/^{12}C$ gradient between the ocean's surface and bottom layers was 25% larger during the last ice age than at present. Broecker (1982) proposed that an increase in the phosphate content of the deep sea could explain these observations. We follow up here on a proposal by Sarmiento and Toggweiler (1984) that glacial to interglacial changes in P_{CO2} are related to changes in the nutrient content of high-latitude surface water. We develop a four-box model of the ocean and atmosphere which includes low- and high-latitude surface boxes, an atmosphere, and a deep ocean. In simplest form the model equations show that the CO_2 content of high-latitude surface water is directly connected to the huge reservoir of CO_2 in deep water through the nutrient content of high-latitude surface water. The relationship between the CO_2 content of low latitude surface water and the deep sea is more indirect and depends to a large extent on transport of CO_2 through the atmosphere from high latitudes. We illustrate how the ^{14}C content of the atmosphere and that of high-latitude surface water constrain model solutions for the present ocean and how ice age ^{13}C observations constrain ice age parameters. We propose that the low ice age P_{CO2} can be produced by a reduction in local exchange between high-latitude surface water and deep water. The model requires that the current exchange rate of about 50 Sv be reduced to about 10 Sv. We review evidence in the geologic record for widespread changes in deep convection around Antarctica about 14,000 years ago which are synchronous with the change in atmospheric P_{CO2}.

Introduction

Three important facts about the chemistry of the ocean and atmosphere during the geologically recent past have come to light in recent years. CO_2 measurements on gas bubbles trapped in glacial ice have shown that the partial pressure of CO_2 in the atmosphere during the last ice age (~18,000 years ago) was about 70 ppm lower than it has been during the interglacial period (beginning ~10,000 years ago) [Neftel et al., 1982]. This is significant because it suggests that global climate changes have been induced, or at least amplified, by changes in the CO_2 content of the atmosphere. Climate projections for the future predict a 2°C rise in temperature with a doubling of atmospheric CO_2 levels [Manabe and Stouffer, 1980]. Lower CO_2 levels in the past are therefore consistent with cooler climates. A CO_2-induced cooling during the ice age explains how glaciations might occur simultaneously in both northern and southern hemispheres in spite of the fact that the Milankovitch orbital forcing favors the growth of ice sheets in one hemisphere but not the other.

The glacial ice also tells us that the P_{CO2} of the atmosphere prior to the period of rapid industrialization was about 270 ± 10 ppm compared to about 345 ppm today [Stauffer et al., 1984]. Therefore, the change in atmospheric CO_2 content since the middle of the last century to the present is about the same as the change between glacial and interglacial periods. Although no obvious climatic changes have been linked to the recent rise in CO_2, most students of climatic change hold that the effects of CO_2 on climate operate through feedbacks in the climatic system involving, for example, changes in water vapor transport or changes in the ice albedo feedback in high latitudes. Because of the flywheel effect of the oceans these processes may take some time to become established [Bryan et al., 1982].

Shackleton [1977], Vincent et al. [1981], and Shackleton et al. [1983a, b] have shown using carbon isotope measurements in deep-dwelling benthic forams that the $^{13}C/^{12}C$ ratio in the deep sea was lower during the ice age than at present. At the same time the ^{13}C content of surface-dwelling planktonic forams seems not to have changed [Shackleton et al., 1983b]. While all the data on isotopic changes in benthic forams seem to support some glacial to interglacial increase in the $\delta^{13}C$

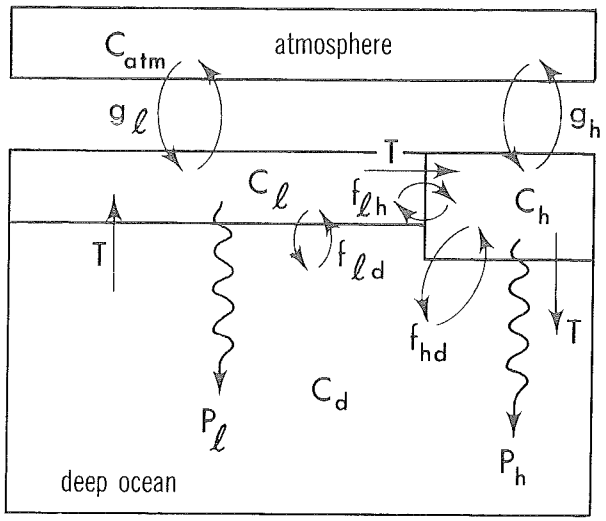

Fig. 1. Schematic diagram of the four-box model.

content of the deep sea, there is uncertainty with regard to the absolute magnitude. Estimates of the magnitude range from barely significant to as much as 0.7 per mil. We assume that the highly resolved 0.5 per mil increase recorded by Shackleton et al. [1983a, b] for core V19-30 in the eastern equatorial Pacific is a representative value. This means that the gradient in $^{13}C/^{12}C$ between the surface and the deep sea increased by 25% over the preindustrial gradient of about 2.0 per mil. This observation suggests that the ice age ocean was more effective at sequestering biologically fixed CO_2 in the deep sea. One can also infer that the oxygen content of the deep sea was lower during the ice age because of the close association between $\delta^{13}C$ and oxygen in the ocean's photosynthesis/respiration cycle.

Broecker [1982] proposed that an increase in the phosphorus to carbon ratio in the glacial deep sea could explain the lower atmospheric P_{CO2} and the carbon isotope changes. He proposed that erosion of organic sediments from exposed continental shelves during the ice age might add extra phosphorus to the ocean. In simplest terms, this hypothesis says that a unit of nutrient-rich deep water upwelling to the surface during the ice age sustains more biological productivity. This enhances the flux of detrital organic carbon from the surface to the deep sea and pulls CO_2 out of the atmosphere. The excess organic carbon in the deep sea, when oxidized by deep-sea organisms, reduces deep-sea oxygen levels and increases the $^{13}C/^{12}C$ gradient between the surface and deep ocean. One consequence of Broecker's shelf erosion hypothesis is that lower atmospheric CO_2 levels must follow the growth of the ice sheets; the proposed ocean chemistry changes can only occur after the sea level has been lowered.

What we propose here is a different model for the CO_2 lowering which shows how changes in the ocean's large-scale circulation can reduce the CO_2 content of the atmosphere independently of continental glaciation and sea level changes. Like Broecker's model, this one calls on changes in ocean nutrient content but not in the deep sea or over the ocean as a whole. This model requires only that changes in the nutrient content in high-latitude surface water be altered. Nutrient levels in present-day high-latitude surface water are quite high, particularly in the Antarctic. We will show that these high nutrient levels are consistent with a well-oxygenated deep ocean. Lower CO_2 levels in the ice age atmosphere are consistent with lower nutrient levels in high-latitude surface water and a poorly oxygenated deep sea. We propose that glacial to interglacial changes in atmospheric CO_2 are probably driven by changes in the dynamics of convection in the Antarctic. Time scales for this transition are short enough that changes in atmospheric P_{CO2} might have played an active role in forcing the end of the last ice age.

The model to be discussed here has been presented in preliminary form by Sarmiento and Toggweiler [1984]. Two other groups, working independently, have published papers using very similar models [Siegenthaler and Wenk, 1984; Knox and McElroy, 1984]. These authors also have papers appearing in this volume [Wenk and Siegenthaler, this volume; Ennever and McElroy, this volume]. We will detail here how the model works and how carbon isotopes constrain model solutions. In the first section below we present

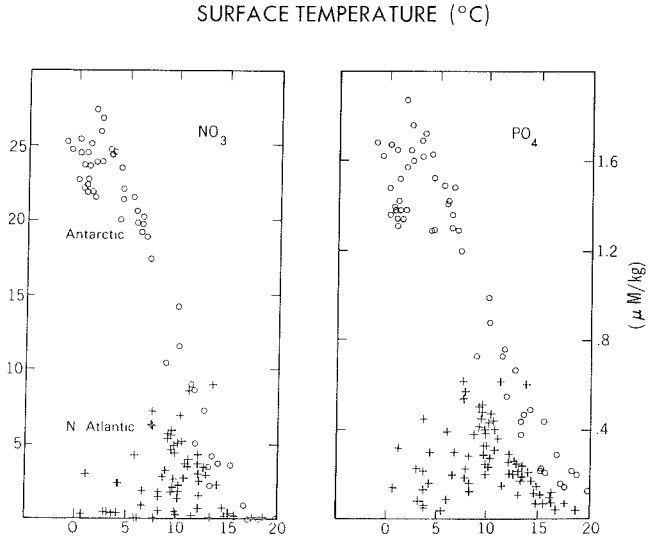

Fig. 2. Nitrate and phosphate content of high-latitude surface water plotted against surface temperature. Antarctic points are plotted as open circles. North Atlantic points are plotted as crosses. GEOSECS and TTO data.

TABLE 1. Stoichiometric Relationships Between Model Variables

	Standard Redfield Ratios[a]	Ratios Used in Model
$\Delta O_2/\Delta P$	-138	-169
$\Delta C_{org}/\Delta P$	106	130
$\Delta \Sigma CO_2/\Delta P$[b]	132.5	162.5
$\Delta Alk/\Delta P$	38	50

[a]Redfield et al. [1962].

[b]Assuming for both cases that 20% of ΣCO_2 increase in deep sea is due to $CaCO_3$ dissolution [Li et al., 1969; Kroopnick, 1974].

a set of idealized model equations which provide the simplest and most illustrative description of the model. In the second and third sections we present model results for the present ocean and ice age ocean, respectively. In the discussion to follow we attempt to relate the model's predictions to what one observes in the real world and examine the evidence for predicted ocean chemistry changes. An appendix follows, in which technical aspects of the model's construction are presented.

The Idealized Model Equations

The model presented here is diagrammed in Figure 1. It differs from a standard geochemical two box ocean model by including a box which represents high-latitude surface water, combining North Atlantic and Antarctic deep water formation regions. C_{atm}, C_ℓ, C_h, and C_d represent the tracer contents of the atmosphere, low-latitude surface water, high-latitude surface water, and the deep ocean, respectively. This model configuration is similar to one developed by Keeling and Bolin [1968] for the Pacific Ocean. Using a data set of much poorer quality than those presently available, Keeling and Bolin attempted with great difficulty to derive fluxes between the boxes from averaged data. In our approach here we will make some simplifying assumptions which Keeling and Bolin did not make. Also, in producing a global model we use the overall atmospheric balances of CO_2 and ^{14}C as model constraints. At the time when Keeling and Bolin developed their model no one had reason to believe that the CO_2 content of the atmosphere had varied so widely in the recent past. Keeling and Bolin, therefore, did not explore the possibilities which we consider here.

We include in the high-latitude box the area of the North Atlantic poleward of 60°N and the areas of the South Atlantic, South Pacific, and Indian Oceans poleward of 50°S. Approximately 15% of the ocean's surface is included in this definition; the area of the ocean south of 50°S is seven times larger than the area of the North Atlantic north of 60°N. The surface of the Arctic Ocean is ignored because ice coverage cuts off exchange between the ocean and atmosphere. The surface boxes ℓ and h are assumed to have average mean annual temperatures of 21.5° and 2.5°C, respectively, as determined from the Levitus [1982] data set. We assume that the low-latitude box is 100 m deep and the high-latitude box is 250 m deep.

The bidirectional arrows labeled g_ℓ and g_h represent gas exchange between the surface boxes and the atmosphere. Peng et al. [1979] found that an average gas exchange piston velocity of about 3 m/day applies over most of the ocean, and we adopt this value for both surface boxes. This does not mean that the gas exchange rates are the same; the effect of temperature on CO_2 solubility makes the high-latitude CO_2 gas exchange rate approximately twice that of the low-latitude box. The wiggly lines labeled P_ℓ and P_h represent particulate phosphorus fluxes from the surface layers to the deep sea.

The bidirectional arrows labeled f_{hd}, $f_{\ell d}$, and $f_{\ell h}$ represent simple first-order water exchange between the boxes indicated by the subscripts. The arrows labeled with a T represent a one-way cycle in which water flows from the low-latitude surface box to the high-latitude box, to the deep ocean box, and back to the low-latitude surface box again. The variable T represents the large-scale thermohaline overturning of the ocean in which warm water flows poleward, cools, sinks into the deep sea, and then upwells back to the warm surface through the ocean's thermocline. Of the bidirectional fluxes, the f_{hd} term connecting high-latitude surface water with the deep sea is by far the most important. It can be thought of as deep convection in high latitudes or as isopycnal mixing along deep density surfaces outcropping at high latitudes. The preliminary report mentioned above [Sarmiento and Toggweiler, 1984] discusses model solutions for ordinary $^{12}CO_2$ in which $f_{\ell d}$ and $f_{\ell h}$ are set equal to zero. We will maintain this simplification throughout this section.

Photosynthesizing ocean plants living in warm ocean surface water are capable of taking up virtually all available nitrate and phosphate and of incorporating these vital nutrients into their body tissues. For this reason the biological productivity of warm surface water can be said to be nutrient limited. When the plants are eaten by grazing zooplankton, the nutrients ultimately find their way into excreted particles which sink out of the photic upper layers. When a unit of deep water upwells into the warm surface ocean, all of the upwelled nitrate and phosphate thus returns to the deep sea in organic form as a component of

TABLE 2. State Variables for the Ocean/Atmosphere System

	Preindustrial Value	Source	Ice Age Value[a]
Volume of the ocean	1.292×10^{18} m^3	Levitus [1982]	1.249×10^{18} m^3
Area of the ocean's surface	3.49×10^{14} m^2	Sverdrup et al. [1942]	same
Mole volume of the atmosphere	1.773×10^{20} moles	Weast and Astle [1979]	same
Average AOU content of the deep sea below upper 100 m (AOU_d)	154 μmol/kg	GEOSECS/TTO	---
Total phosphate content of the ocean	2.77×10^{15} moles (avg = 2.09 μmol/kg)	GEOSECS/TTO	same
Total alkalinity content of the ocean	3.140×10^{18} eq. (avg = 2371 μeq/kg)	GEOSECS/TTO	3.267×10^{18} equivalents
Total ΣCO_2 content of the ocean	2.990×10^{18} moles (avg = 2258 μmol/kg)	GEOSECS/TTO	---
Average $\delta^{13}C$ of the ocean	0.55 per mil	Broecker and Peng [1982][b]	--
Average $[^{14}C]$ of the ocean	2.27×10^{-15} moles/kg (85.1% of atmospheric equilibrium)	Stuiver et al. [1981][c]	--
Total ΣCO_2 content of the ocean and atmosphere	3.0245×10^{18} moles	---d	3.1517×10^{18} moles
Total $\Sigma^{13}CO_2$ content of ocean and atmosphere	3.0263×10^{18} moles $\cdot {}^{13}C/{}^{12}C_{stnd}$	---e	3.1521×10^{18} moles $\cdot {}^{13}C/{}^{12}C_{stnd}$
Total $\Sigma^{14}CO_2$ content of ocean and atmosphere	2.5578×10^{18} moles $\cdot {}^{14}C/{}^{12}C_{stnd}$	---f	2.6182×10^{18} moles $\cdot {}^{14}C/{}^{12}C_{stnd}$
Depth of the low-latitude surface box	100 meters		same
Depth of the high-latitude surface box	250 meters		same
Temperature and salinity of the low-latitude surface box	21.5°C, 34.7 mg/g		20.0°C, 35.9 mg/g
Temperature and salinity of the high-latitude surface box	2.5°C, 34.7 mg/g		2.0°C, 35.9 mg/g

[a]Ice age state variables have been determined as follows: for the ocean volume we assume that enough fresh water leaves the ocean to increase salinity from 34.7 to 35.9 per mil following Broecker [1982]; we add 1.272×10^{17} moles of isotopically light (−23 per mil) carbon to the system (this is sufficient to decrease the deep ocean $\delta^{13}C$ by 0.5 per mil); we then add an equal amount of alkalinity and isotopically neutral (0 per mil) ΣCO_2 to the system to simulate $CaCO_3$ dissolution from the seafloor; we assume that half of the added ΣCO_2 is terrestrial

sinking particles. In terms of the diagram in Figure 1 we can write

$$P_{\ell} = PO4_d \cdot T \quad (1)$$

where only the major water flux terms, f_{hd} and T, are considered. To avoid confusion regarding subscripts, we will not subscript molecular formulas in expressions in which model subscripts appear. For example, we will use $PO4_d$ in place of PO_{4d}.)

When the same unit of deep water upwells to the surface, the CO_2 content of the water is reduced in proportion to the phosphorus removal as organic tissues are formed. The molar ratio of C to P taken up is known as the Redfield ratio and is traditionally given the value 106:1 [Redfield et al., 1962]. Following Broecker [1982], we will use phosphate as a representative, idealized limiting nutrient. We could easily choose to use nitrate in the same manner. Nitrate is thought to be more limiting in the ocean than phosphate; however, it has some small non-Redfieldian sources and sinks within the ocean which are not well quantified.

The Redfield ratio which links phosphorus and nitrogen to carbon in fixed proportions is based on measurements of C:P and C:N ratios in live ocean plants sieved from surface water. It is normally assumed that these ratios hold for organic particulate matter throughout the water column. Evidence from particle traps, however, suggests that organic phosphorus and nitrogen are remineralized more rapidly than organic carbon [Knauer et al., 1979; Honjo, 1980]. Therefore, the ratios of C:P or C:N are larger in particles which are destroyed in the deep sea, as opposed to those destroyed in the upper ocean. Indeed, Takahashi et al. [1984] show that relative changes in oxygen and phosphorus along intermediate water density surfaces follow an average slope of -172 ± 6:1. Given the Redfield ratio of 1.3 moles O_2 consumed per mole organic carbon oxidized, this slope translates into a C:P ratio of about 130:1.

For the high latitude surface box we can write the following equation:

$$P_h = PO4_d \cdot f_{hd} - PO4_h \cdot (T+f_{hd}) \quad (2)$$

where again the particle flux P_h refers to the downward flux of phosphorus and the flux terms $f_{\ell d}$ and $f_{\ell h}$ are ignored.

If we assume that the oxygen content of the two surface boxes is always in equilibrium with the atmosphere, we can write an equation describing the deep-ocean oxygen content as a function of P_{ℓ} and P_h. Here, we express the oxygen content in terms of the apparent oxygen utiliztion (AOU), which is the difference between the dissolved oxygen concentration at saturation (a function of water temperature) and the measured oxygen concentration. We assume here that the AOU of the two surface boxes is zero.

$$AOU_d = r_{O2:P} \cdot (P_{\ell}+P_h)/(T+f_{hd}) \quad (3)$$

Table 2 (continued)

biomass with a $\Delta^{14}C$ of -50 per mil; the other half is assumed to be dead with respect to ^{14}C.

[b]The average $\delta^{13}C$ for the world ocean is estimated using the correlation between $\delta^{13}C$ and PO_4 given by Broecker and Peng [1982] Figure 6-12, p. 309 and the average PO_4.

[c]A subtle, but important, error exists in the Stuiver et al. [1981] compilation. Although the reported average ^{14}C concentration units for the various ocean basins are given as moles per cubic meter, the figures and tables actually have units of moles per 1000 kg. One must multiply Stuiver et al.'s [1981] ^{14}C concentrations by 1.025 before comparing ^{14}C with ^{12}C in units of moles per cubic meter. Otherwise an error of 10-15% will result with respect to the amount of ^{14}C decay or "aging" one would predict for the ocean relative to the atmosphere.

[d]The total ΣCO_2 content of the preindustrial ocean and atmosphere is the sum of the total ΣCO_2 for the ocean given above plus the atmospheric CO_2 content in 1973 (320×10^{-6} atm times 1.773×10^{20} moles of air) less twice the fossil fuel CO_2 input through 1973 (11×10^{15} moles [Broecker and Peng, 1982]). We have assumed that a terrestrial biomass release equal to the fossil fuel release has entered the atmospheric during the last century.

[e]The total $\Sigma^{13}CO_2$ content of the preindustrial ocean and atmosphere is calculated as in note d above, where the ocean $\delta^{13}C$ is +0.55 per mil, the atmosphere $\delta^{13}C$ is -7.2 per mil, and the subtracted fossil fuel/biomass $\delta^{13}C$ is -26 per mil. The number of significant digits reported in the carbon isotope totals reflects relatively small isotopic shifts between the tracers.

[f]The total $\Sigma^{14}CO_2$ content of the preindustrial/prebomb ocean and atmosphere is computed in similar manner to ^{13}C above where the 1973 atmosphere is 450 per mil enriched in ^{14}C and the released biomass ^{14}C is assumed to be -60 per mil (the fossil fuel component contains no ^{14}C). We subtract 8.42×10^4 moles of bomb ^{14}C from the total. This total is derived from the 314×10^{26} bomb ^{14}C atoms reported by Broecker et al. [1980] to be residing in the ocean in 1973 and from the 480 per mil of bomb ^{14}C in the atmosphere (450 per mil plus 30 per mil for compensation of the Seuss effect).

The term $r_{O2:P}$ is the ratio of oxygen consumed to phosphate regenerated when organic matter is oxidized. We also assume in equation (3) that all particulate organic matter falling into the deep box is oxidized. In other words, none of the particulate flux is lost to the sediments.

We can now combine equations (1), (2), and (3) and write an expression for the phosphate content of high-latitude surface water:

$$PO4_h = PO4_d - AOU_d/r_{O2:P} \quad (4)$$

We see from equation (4) that the nutrient content of high-latitude surface water is directly linked to the oxygen content of the deep sea; i.e., a well-oxygenated deep sea coexists with high nutrient levels in high-latitude surface water. Since the average phosphate concentration of the deep sea is about 2.15 μmol/kg and the average AOU is about 154 μmol/kg, we calculate a $PO4_h$ of 1.24 μmol/kg. Nutrients in newly formed deep water are often referred to as "preformed nutrients"; here, $PO4_h$ is the same as preformed phosphate.

Figure 2 shows the nitrate and phosphate contents of high-latitude (summer) surface water plotted against temperature. The circles represent Antarctic locations, while the pluses represent the North Atlantic. The nutrient contents of Antarctic and North Atlantic surface waters climb above near-zero mid-latitude values at temperatures below 15°C. Antarctic nutrient values increase to much higher values than those found in the North Atlantic. Our preformed phosphate concentration of 1.24 μmol/kg plots just below the cluster of Antarctic points.

In high latitudes, far more nutrients are delivered to the surface than can be utilized by plants. High-latitude surface water is not underlain by the intense thermocline found at lower latitudes; in winter the water column is often able to convect to great depth, bringing nutrient-rich deep water to the surface. Over much of the year there is insufficient light to support plant growth, so nutrients go unutilized. Because we define our high-latitude box to be that region of the surface ocean in which nutrient levels are non-zero, we can use the information in Figure 2 as a rough guide in demarcating the box's latitudinal extent. The midpoint of the Antarctic nutrient rise is found at about 10°C. If we take the 10° summer isotherm as our boundary, the high-latitude box is defined as the ocean area poleward of 50°S in the Antarctic and 60°N in the North Atlantic.

It is instructive to consider what would happen if there were no high-latitude region in the ocean. If, somehow, warm surface water (with preformed $PO_4 = 0$) were to be taken directly to the deep ocean and allowed to upwell back to the surface, phosphate could enter into the deep sea only in the form of organic particles. Looking at the oxygen balance, one finds that the oxygen demand of such a particle flux depletes the deep ocean of oxygen, even if one allows the downwelling water to become saturated with oxygen at deep-ocean temperatures. Expressed mathematically,

$$O2_d = O2_{sat}(T) - r_{O2:P} \cdot PO4_d \quad (5)$$

The saturation oxygen content at the average temperature of the deep sea is approximately 325 μmol/kg. Given $PO4_d$ = 2.15 μmol/kg and $r_{O2:P}$ = 169, one calculates that the oxygen demand from the phosphate flux is greater than the oxygen content of newly formed deep water. This situation is not observed in the ocean today; the average oxygen content of the deep sea is about 170 μmol/kg. Therefore, the deep sea is not depleted in oxygen to even half its saturation content. The real ocean shunts much of the upward flux of phosphate to high-latitude regions, allowing phosphate to reach the surface outside of the domain of the warm surface ocean. In high latitudes the deep sea's oxygen content is replenished without upwelled phosphate generating a tremendous organic particle demand on the deep-ocean oxygen content.

For the other tracers we want to study with this model (ΣCO_2, alkalinity, ^{13}C, and ^{14}C) the equations describing their steady state distributions among the four boxes in Figure 1 will be more complicated. There are no simplifying assumptions to be made regarding surface water as there are with phosphate and oxygen. One must also contend with exchanges between the ocean and atmosphere. There is, however, one simple relationship we can construct. Again ignoring $f_{\ell d}$ and $f_{\ell h}$, we can write the following equation for total CO_2 in the deep box:

$$\Sigma CO2_d \cdot (T+f_{hd}) = \Sigma CO2_h \cdot (T+f_{hd}) + r_{\Sigma C:P} \cdot (P_\ell + P_h) \quad (6)$$

Here, $r_{\Sigma C:P}$ represents the ratio of total carbon (including $CaCO_3$) to phosphate in sinking particulate matter. We assume a constant fraction of four parts organic carbon to one part carbonate in particulate matter as originally proposed by Li et al. [1969] and later supported by Kroopnick [1974]. We then express $r_{\Sigma C:P}$ in terms of the C:P ratio in organic matter as follows:

$$r_{\Sigma C:P} = \frac{r_{C_{org}:P}}{(1-f_{Ca})} = \frac{130}{0.8} = 162.5 \quad (7)$$

where f_{Ca} is the carbonate fraction of the total carbon flux. Rearranging and substituting equations (1) and (2) into (6), we arrive at the following result:

$$\Sigma CO2_h = \Sigma CO2_d - r_{\Sigma C:P} \cdot (PO4_d - PO4_h) \quad (8)$$

Rearranging again, we find

$$\frac{\Sigma CO2_d - \Sigma CO2_h}{PO4_d - PO4_h} = r_{\Sigma C:P} \quad (9)$$

Equation (9) states that the relative differences in ΣCO_2 and phosphate between high-latitude sur-

face water and deep water are given simply by a constant ratio. One can derive a similar relationship for alkalinity, where the constant relating alkalinity to phosphorus is given by

$$r_{Alk:P} = 2 \cdot f_{Ca} \cdot r_{\Sigma C:P} - r_{N:P} \quad (10)$$

$r_{Alk:P}$ has a value of 50 when we substitute the constants cited above. We assume $r_{N:P}$ has a value of 15. Table 1 summarizes the stoichiometric relationships between oxygen, alkalinity, carbon, and phosphorus used in this study.

Equation (9) is a very significant result. The high-latitude ΣCO_2 and alkalinity together determine the P_{CO2} of high-latitude surface water. Because both of these quantities are anchored to deep-sea values, this result says, in effect, that the CO_2 content of the atmosphere is anchored to the deep sea through the nutrient content of high-latitude surface water. The relationship between the P_{CO2} of low-latitude surface water and the deep sea is more indirect, depending on transport of CO_2 through the atmosphere from high-latitudes.

One can calculate a value of $r_{\Sigma C:P}$ using equation (9) in order to test the applicability of our C:P ratio of organic matter. We have computed average ΣCO_2 and phosphate values for the deep sea of 2257 μmol/kg and 2.15 μmol/kg, respectively (Table 2). Averaging all the surface Geochemical Ocean Sections Study (GEOSECS) data for the Antarctic south of 50° while normalizing to the deep-sea salinity, we find $\Sigma CO2_h$ = 2178 ± 10 μmol/kg and $PO4_h$ = 1.51 μmol/kg. We assume that Antarctic surface water contains ~25 μmol/kg of fossil fuel CO_2 and subtract this from $\Sigma CO2_h$. (A 50-ppm excess of fossil fuel CO_2 in the atmosphere becomes a ΣCO_2 excess of 25 μmol/kg in surface water using a buffer factor of 14.) Substituting into equation (9), we find that $r_{\Sigma C:P}$ = 150-175. This result roughly confirms the number predicted, 162.5, from Takahashi et al.'s [1984] observations of O_2:P. The standard Redfield ratio of 106 units organic carbon to one unit phosphorus represents a total carbon to phosphorus ratio of only 132.5 using equation (7).

Before solving the full set of equations for ΣCO_2, alkalinity, and the carbon isotopes for all four boxes, we write a set of conservation equations which express the deep-box tracer concentrations as functions of the total amount of tracer in the ocean and atmosphere. As an example we write out the conservation equation for ΣCO_2 below:

$$\Sigma CO2_d = (\Sigma CO2_T - \Sigma CO2_h \cdot V_h - \Sigma CO2_\ell \cdot V_\ell - P_{CO2} \cdot V_{atm})/V_d \quad (11)$$

$\Sigma CO2_T$ is the total amount of carbon in the ocean and atmosphere in units of moles C. The terms V_h, V_ℓ, V_{atm}, and V_d represent the volumes of the subscripted boxes. The volume of the atmosphere is expressed as moles of gas molecules such that the product of the P_{CO2} (a mixing ratio) and the mole volume of the atmosphere has units of moles CO_2. Conserving total tracer content ensures that the present-day partitioning of tracers will not influence model solutions for other possible scenarios.

We have averaged all the GEOSECS and Transient Tracers in the Ocean (TTO) data within 5° latitude belts at standard National Oceanographic Data Center (NODC) levels and added the belts together to produce total tracer contents for the ocean. The results appear in Table 2. The validity of using conservation expressions like equation (11) in our model is compromised by the fact that the ocean and atmosphere are not presently at steady state with respect to ΣCO_2, ^{13}C, and ^{14}C; modern additions of fossil fuel CO_2 and bomb ^{14}C have perturbed the presumed steady state which existed prior to industrialization. We account for this by simply subtracting the added quantities from the totals. The addition of unknown amounts of terrestrial biomass carbon to the atmosphere makes this correction somewhat imprecise; the maximum errors, however, are not large.

Before proceeding we would like to introduce an additional observation into the model regarding the degree of oxygen saturation in newly formed deep-water masses. Weiss et al. [1979] report that the oxygen content of remnant Weddell Winter Water and Weddell Shelf Water during the summer is about 40 μmol/kg undersaturated. Gordon et al. [1984] report that the oxygen content of Antarctic surface water under sea ice at the end of the austral winter is 45 μmol/kg undersaturated (86% of saturation). Gordon et al. argue that the 14% undersaturation has not been appreciably altered by biological processes over the winter period. These observations are characteristic of oceanographic observations in deep-water formation regions: nowhere are subsurface water masses in these regions less than 10% undersaturated. Because the process of oxygen equilibration takes a finite amount of time (one month for a 100-m mixed layer) it is not hard to imagine that a convectively unstable water mass might not aquire its full measure of oxygen.

The above observations are suggestive that newly formed deep water is not fully saturated with oxygen. If newly formed deep water carries an initial oxygen deficit into the deep sea, the oxygen deficit of average deep water due to oxidation of organic matter is reduced accordingly. We will make an assumption that the model's AOU_h is 10% undersaturated and will consider this to be a much better choice than AOU_h = 0. A 10% undersaturation in newly formed deep water reduces the deep-sea oxygen deficit caused by the oxidation of organic matter by 30 μmol/kg, nearly a 20% reduction. A 10% undersaturation in AOU_h also increases the predicted $PO4_h$ or preformed phosphate to 1.41 μmol/kg (see equation (12) below). Referring back to Figure 2, we find that the predicted $PO4_h$ is inside the field of Antarctic data. The model equations in the appendix include an AOU_h term.

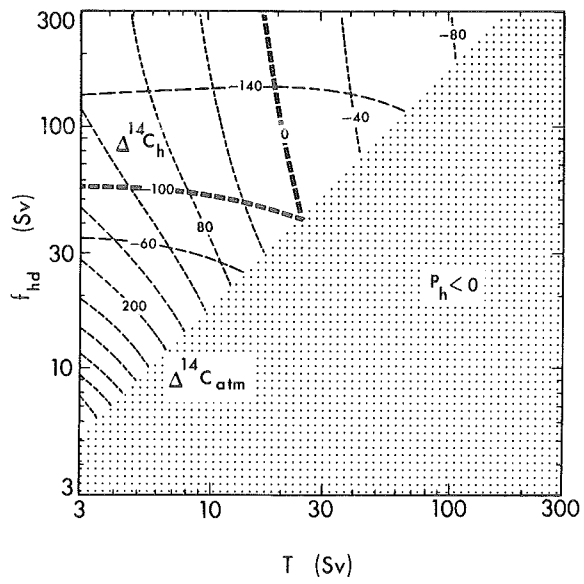

Fig. 3. Contour plot of model results for the ^{14}C contents of the atmosphere, $\Delta^{14}C_{atm}$, and high-latitude surface water, $\Delta^{14}C_h$, in the parameter space of high-latitude convection (f_{hd}) versus thermohaline overturning (T). Contours for atmospheric $\Delta^{14}C$ are the diagonally trending dashed lines labeled as -80, -40, etc. starting from the upper right. Contours for high-latitude surface water are the horizontally trending dashed lines labeled -140, -100, and -60. The heavy contour lines represent contours for $\Delta^{14}C_{atm}$ = 0 and $\Delta^{14}C_h$ = -100 per mil. Horizontal and vertical axes are log scales. The contours are constructed from 440 model runs evenly spaced over the parameter range. The model run in this figure represents the simple case in which $f_{\ell d}$ and $f_{\ell h}$ are set to zero. AOU_d = 154 µmol/kg, AOU_h = 30 µmol/kg, and $r_{\Sigma C:P}$ = 162.5. The stipled region represents the region of the parameter space in which P_h is less than zero (see text).

A Model Solution For The Present Ocean

Our point of departure for describing the present ocean is to use the observed AOU_d and the assumed AOU_h to determine the particle fluxes into the deep sea. We can then use the partitioning of ^{14}C between the various boxes to limit the flux terms, f_{hd} and T. Later in this section we will investigate the role of $f_{\ell d}$. As we see in equation (12),

$$PO4_h = \frac{(T+f_{hd}+f_{\ell d})}{(T+f_{hd})} \cdot (PO4_d - \frac{AOU_d}{r_{O2:P}}) + \frac{AOU_h}{r_{O2:P}} \qquad (12)$$

knowing AOU_d and AOU_h allows one to predict the phosphate content of high-latitude surface water as a function of T, f_{hd}, and $f_{\ell d}$. Knowing $PO4_h$ in turn yields P_ℓ and P_h, the particulate phosphate fluxes (equations (1) and (2)). Equation (12) is simplified from equation (A4) in the appendix. We have left out the conservation and $PO4_\ell$ terms, which have little impact in the present illustration.

Two facts are known about the preindustrial and prebomb ocean and atmosphere with regard to ^{14}C. We know that the $\Delta^{14}C$ content of the atmosphere was zero per mil. We also know that the average ^{14}C content of Antarctic surface water was -100 ± 20 per mil from oceanic ^{14}C measurements made prior to the bomb tests [Broecker and Peng, 1982, p. 415]. (We also know the ^{14}C content of low-latitude surface water from coral measurements; however, low-latitude $\Delta^{14}C$ mainly tracks the atmosphere and proves redundant in the present applications.) Throughout the remainder of the paper we will plot model results as contours in a parameter space defined by the major flux terms, f_{hd} and T. High-latitude convection (f_{hd}) and thermohaline overturning (T) affect the partitioning of ^{14}C between the model boxes in different ways such that contours of atmospheric $\Delta^{14}C$ and high-latitude surface water $\Delta^{14}C$ intersect and define a solution for today's ocean.

Model results for the preindustrial ocean and atmosphere appear in Figures 3, 4a-4d, and 5a-5c. Figures 3 and 4 present the simple case in which $f_{\ell d}$ and $f_{\ell h}$ are set equal to zero. Figure 5 examines the effect of varying $f_{\ell d}$ with $f_{\ell h}$ held constant. Each figure represents over 400 model runs in which f_{hd} and T are varied over two orders of magnitude. The scales for f_{hd} and T are identical; each is a log scale in transport extending from 3 to 300 Sv (1 Sv = 10^6 m/s).

In Figure 3, isolines for the preindustrial ^{14}C contents of the atmosphere and high-latitude surface water are drawn in the f_{hd} versus T parameter space. $\Delta^{14}C_{atm}$ values in the upper right-hand corner of the diagram are close to -80 per mil, whereas those in the lower left are greater than +400 per mil. We see that values of $\Delta^{14}C_{atm}$ decrease away from the lower left-hand corner as both f_{hd} and T increase. The flux terms f_{hd} and T act together to ventilate the deep sea. When both are small (lower left-hand part of Figure 3), ^{14}C produced in the atmosphere tends to remain there. When both are large (upper right), the great reservoir of low ^{14}C in the deep sea is able to dilute the atmosphere's ^{14}C production and bring the atmospheric $\Delta^{14}C$ down.

We show three contours of $\Delta^{14}C$ in high-latitude surface water in Figure 3: -60, -100, and -140 per mil. As one might expect, the $\Delta^{14}C_h$ is especially sensitive to exchange between high-latitude surface water and deep water. When f_{hd} is large, the deep ocean is able to pull $\Delta^{14}C_h$ further from atmospheric values.

The point where the $\Delta^{14}C_h$ = -100 isoline meets the $\Delta^{14}C_{atm}$ = 0 isoline defines today's ocean in the f_{hd} versus T parameter space. In Figure 3 the intersection of the ^{14}C lines occurs at the boun-

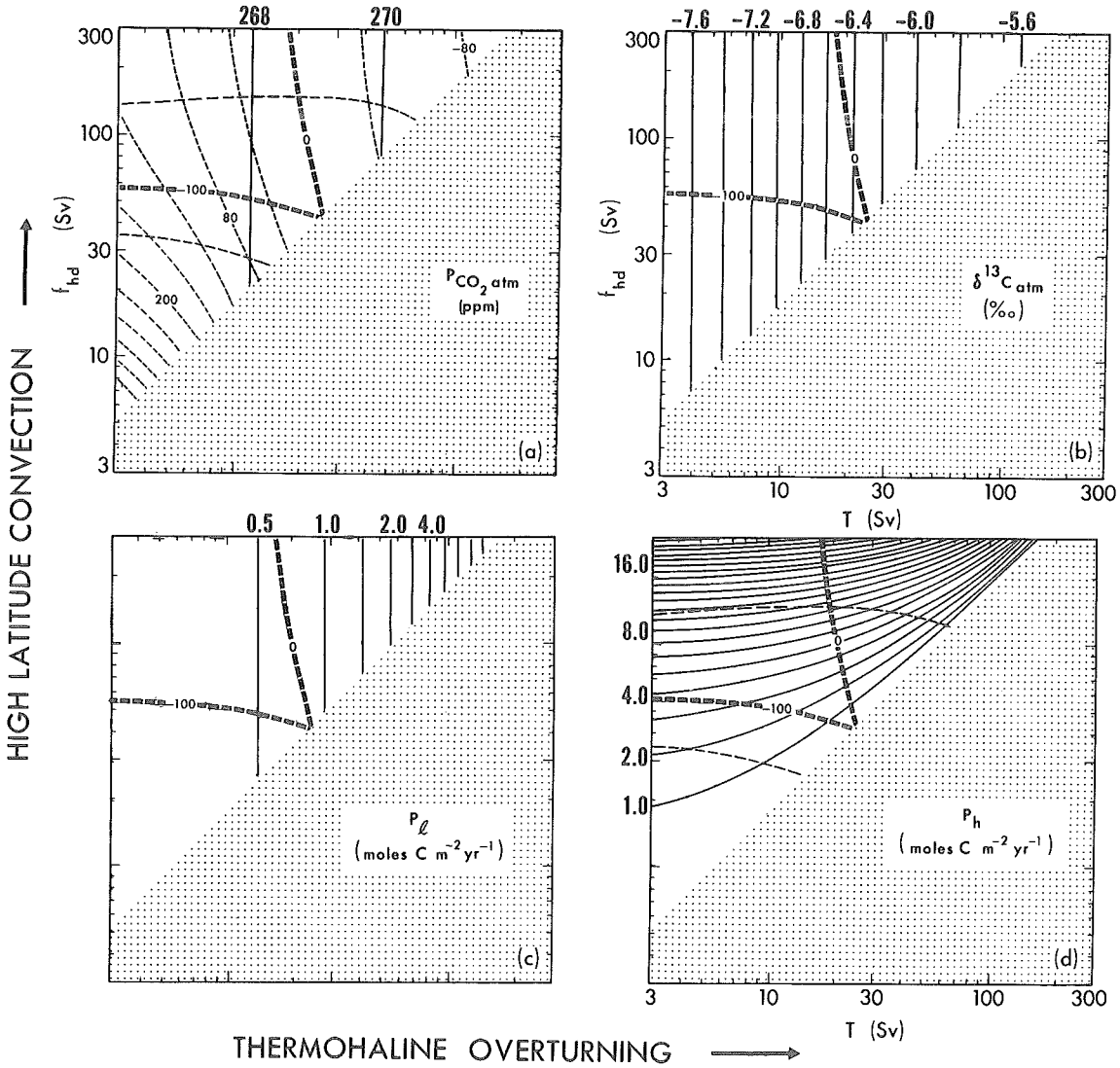

Fig. 4. Contour plots for (a) atmospheric P_{CO2}, (b) $\delta^{13}C_{atm}$, (c) P_ℓ, and (d) P_h overlying the same parameter space and ^{14}C contours shown in Figure 3. Phosphate particle fluxes, P_ℓ and P_h, have been multiplied by $r_{\Sigma C:P}$ (162.5) in Figures 4c and 4d in order to present results in units of moles C per square meter per year (organic plus $CaCO_3$).

dary of the shaded region where f_{hd} is 43 Sv and T is 24 Sv. Given the uncertainty in our knowledge of the preindustrial $\Delta^{14}C$ value for average high-latitude surface water, f_{hd} for today's ocean could be as low as 30 Sv or as high as 75 Sv.

A little more than half of the diagram is shaded, indicating that the high-latitude phosphate particle flux, P_h, in that part of the parameter space is less than zero. It is not difficult to understand why P_h becomes negative over much of the parameter space given the AOU_d restriction. P_ℓ and P_h, when converted to organic carbon fluxes, must sum to produce the deep-sea oxygen deficit (equation (3)). Because the low-latitude area is much larger than the high-latitude area, P_ℓ represents a much bigger drain on the deep-sea oxygen levels than P_h. P_ℓ increases as T increases (equation (1)), and even though T brings oxygen into the deep sea, the particle flux from low-latitude surface water negates it. High-latitude exchange with deep water adds much more oxygen to the deep sea than the high-latitude particle flux can remove. Therefore, when T is large relative to f_{hd}, the particle flux from low-latitude surface water can, by itself, account for more than the observed oxygen deficiency in the deep sea, and P_h is forced to be negative. Note that when $f_{\ell d} = 0$ in equation (12)

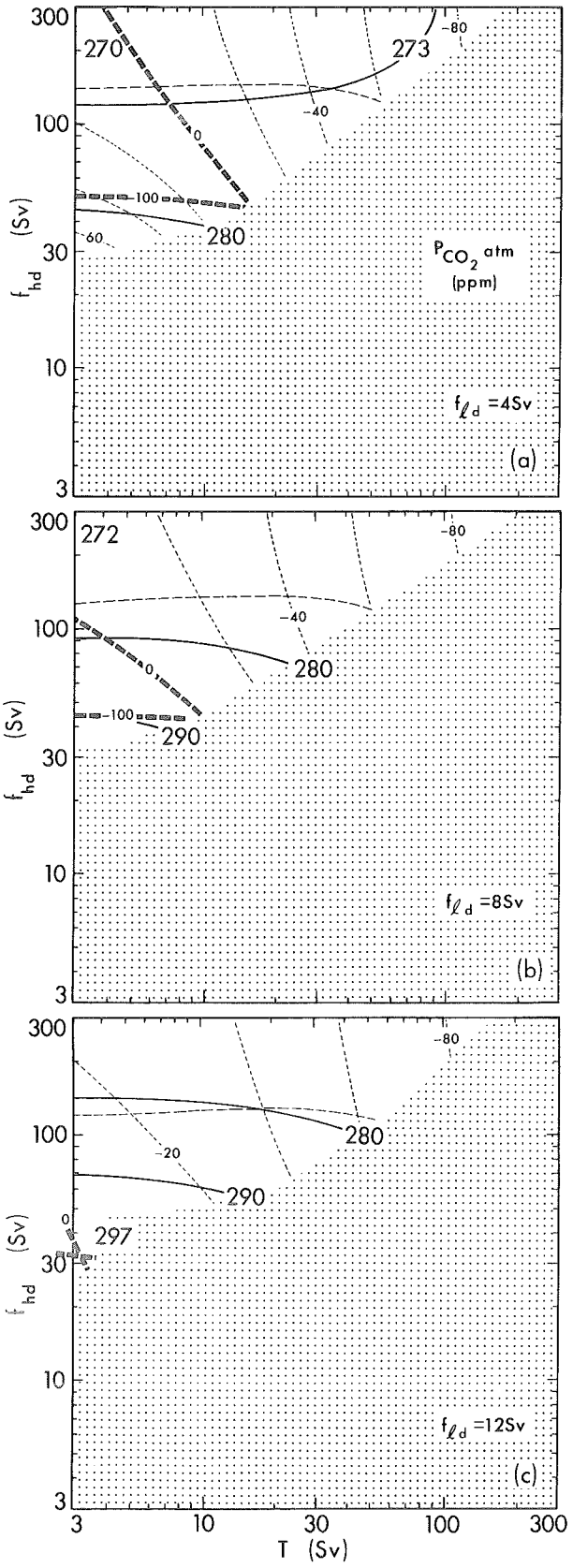

Fig. 5. Contours of atmospheric P_{CO2} (solid lines), $\Delta^{14}C_{atm}$ (short-dashed lines), and $\Delta^{14}C_h$ (longer-dashed lines) in the the same parameter space shown in Figures 3 and 4, but where $f_{\ell d}$ varies from 4 to 12 Sv. Here $f_{\ell h}$ is held fixed at 10 Sv. The $\Delta^{14}C$ contours for 0 per mil in the atmosphere and -100 per mil in high-latitude surface water are accentuated as before. In Figure 5c ($f_{\ell d}$ = 12 Sv) the intersection of the ^{14}C isolines occurs in the stipled region along the left-hand side of the figure. AOU_d = 154 µmol/kg, AOU_h = 30 µmol/kg, and $r_{\Sigma C:P}$ = 162.5.

and AOU_d is held constant, $PO4_h$ is independent of f_{hd} and T. $PO4_h$ equals 1.41 µmol/kg at every point on this diagram.

In Figure 4 the ^{14}C isolines from Figure 3 are used as a base plot over which contours of the atmospheric P_{CO2} (Figure 4a), $\Delta^{14}C_{atm}$ (Figure 4b), P_ℓ (Figure 4c), and P_h (Figure 4d) are plotted. The particle fluxes in Figures 4c and 4d are here converted to total carbon fluxes (organic + carbonate) in units of moles C per square meter per year.

In Figure 4a the atmospheric P_{CO2} isolines plot as vertical lines with the P_{CO2} increasing slightly with increasing T. At the intersection of the $\Delta^{14}C_{atm}$ = 0 and $\Delta^{14}C_h$ = -100 isolines, the P_{CO2} of the atmosphere is 268.8 ppm, well within the estimated range of the preindustrial P_{CO2}, 270 ± 10 ppm [Stauffer et al., 1984]. Fixing AOU_d over the whole parameter space limits the range of atmospheric P_{CO2}'s that we see in Figure 4a. The atmospheric P_{CO2} represents an average of the two surface ocean P_{CO2}'s which are weighted with respect to differential areas and gas exchange rates. At the intersection of the ^{14}C isolines in Figure 4a the P_{CO2} of the low-latitude box is 269.6 ppm, while that of the high-latitude box is 266.5. Free exchange of CO_2 through the atmosphere dampens potential P_{CO2} differences larger than those seen here. If the oxygen content of newly formed deep water were fully saturated (AOU_h = 0), the predicted P_{CO2}'s would be about 25 ppm lower.

In Figure 4b we see contours of the atmospheric ^{13}C content overlying the $\Delta^{14}C$ isolines. At the intersection of the preindustrial ^{14}C isolines, $\delta^{13}C_{atm}$ equals -6.3 per mil as opposed to about -7.6 per mil today. The atmospheric $^{13}C/^{12}C$ composition becomes heavier with increasing T, but shows no sensitivity with respect to f_{hd}. This situation is analogous to the one in Figure 4a. As the thermohaline overturning (T) increases, the flux of carbon in the advective flow through both surface boxes increases relative to the gas exchange fluxes. The effect is more limiting in the high-latitude box because its volume is so much smaller. Cooler temperatures in the high-latitude box favor an equilibrium in which the gas phase is isotopically lighter; warmer temperatures in the low-latitude box favor an isotopically heavier gas phase. Therefore, the atmosphere's

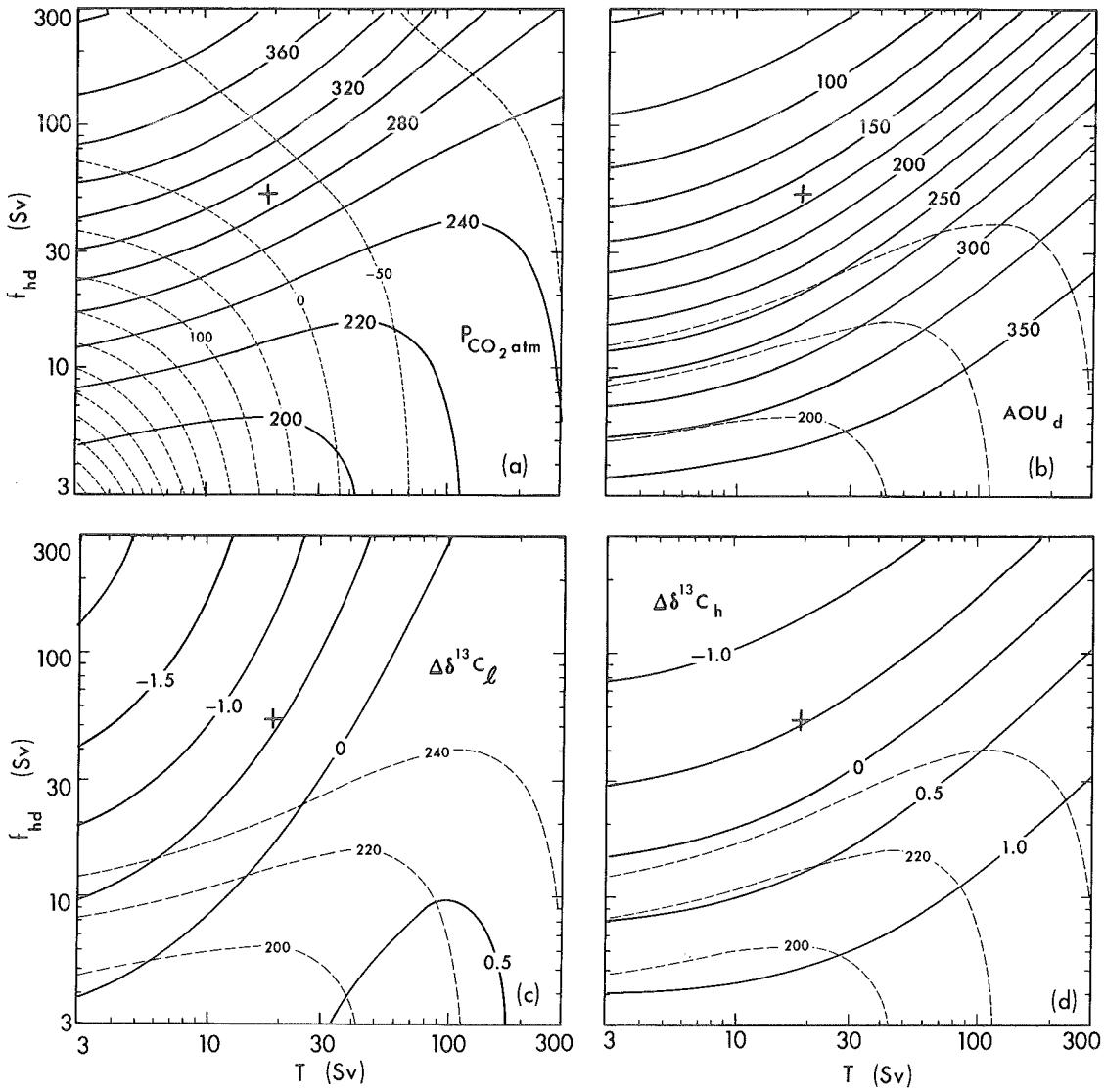

Fig. 6. Model simulation of the last ice age where we have assumed that 51.5 μmol/kg of isotopically light carbon (-26 per mil) has invaded the deep ocean. This input of carbon is sufficient to lower the $\delta^{13}C$ of the deep sea by about 0.5 per mil. We assume that an equal number of moles of $CaCO_3$ dissolves from the seafloor to balance the pH. In this figure the AOU of the deep sea is allowed to vary while the particle flux from high-latitude surface water is fixed at 0.5 moles C m^{-2} yr^{-1}. The plus in each figure part marks the position in f_{hd} versus T parameter space which yields the optimal model solution for the present ocean discussed in the text. The contours shown in Figure 6a are atmospheric P_{CO2} (solid lines) and $\Delta^{14}C_{atm}$ (dashed lines). Contours of AOU_d are plotted in Figure 6b. In Figures 6c and 6d are plotted the difference in $\delta^{13}C$ between the ice age and present (preindustrial) for the low-latitude and high-latitude surface boxes, respectively. In Figures 6b through 6d contours of atmospheric P_{CO2} at 200, 220, and 240 ppm (dashed lines) are carried over from Figure 6a.

$\delta^{13}C$ is driven toward heavier values when T is large. Because the time required to equilibrate the ^{13}C isotopic composition between surface ocean and atmosphere is 10 times longer than the time required to equilibrate CO_2 chemically [Broecker and Peng, 1974], the effect of surface layer flushing with respect to the parameter T is much larger for ^{13}C in Figure 4b than it is for P_{CO2} in Figure 4a.

Figures 4c and 4d show the particulate carbon fluxes out of the surface boxes as functions of f_{hd} and T. As we expect from equation (1), P_ℓ,

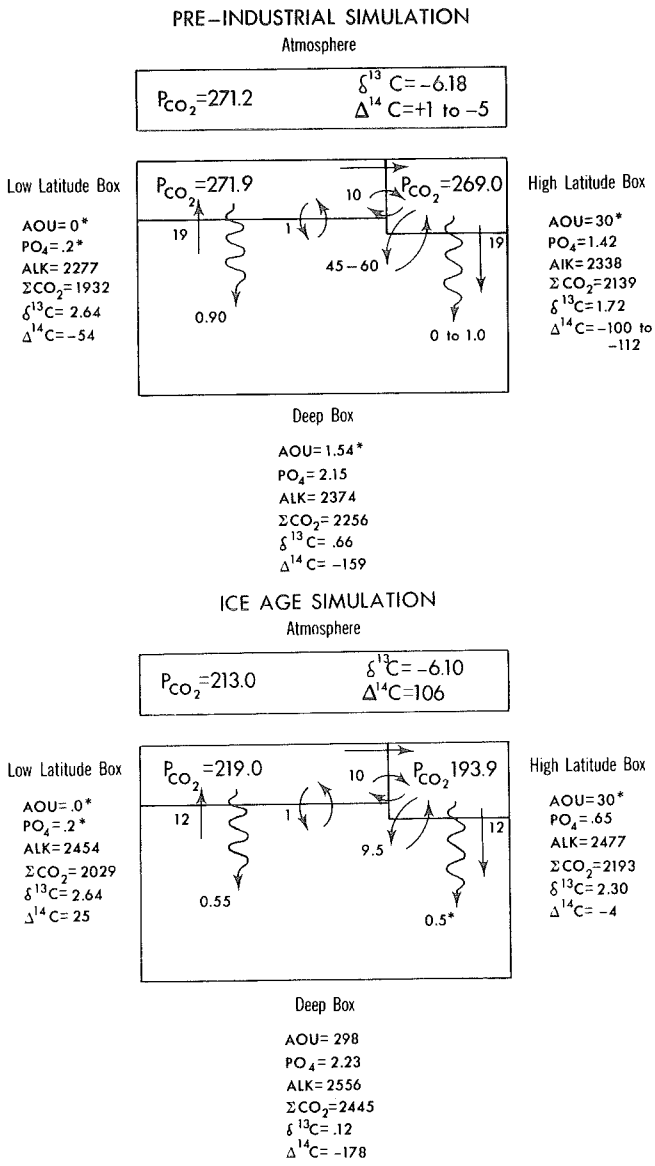

Fig. 7. Steady state concentrations of model variables in the ocean and atmospheric boxes for the preindustrial and ice age simulations. Units are micromoles per kilogram for AOU, PO_4, and ΣCO_2; microequivalents per kilogram for alkalinity, parts per million for P_{CO2}; and parts per thousand (per mil) for $\delta^{13}C$ and $\Delta^{14}C$. Model transports between boxes are given in units of sverdrups (10^6 m^3/s). Particle fluxes are given next to the wiggly arrows in units of moles C per square meter per year. Asterisks indicate values that are initial assumptions.

expressed here as a carbon flux, increases proportionately with T. At the intersection of the preindustrial $\Delta^{14}C$ isolines, P_ℓ has a value of 0.82 moles C m^{-2} yr^{-1}. P_h in Figure 4d is sensitive primarily to f_{hd}. At the intersection of the bold $\Delta^{14}C$ isolines, P_h has a value very close to zero. However, given the range of uncertainty in $\Delta^{14}C_h$ of -80 to -120 per mil, P_h could lie anywhere between -1 and +3 moles C m^{-2} yr^{-1}. High-latitude regions are usually thought to more biologically productive than low-latitude regions. All of the primary productivity measurements in high latitudes, however, reflect summertime conditions. More than half the area of the Antarctic south of 50°S is covered by sea ice in the winter [Burckle et al., 1982]. Winter sea ice, combined with low light levels and deep mixed layers, precludes biological activity over half the year. One could argue that the particle flux from high-latitude surface water, on an annually averaged basis, may not be much different from the particle flux in warmer regions of the ocean [Walsh, 1969]. A high-latitude particle flux of 1.0 moles C m^{-2} yr^{-1} is consistent with a high-latitude preindustrial $\Delta^{14}C$ content of about -110 per mil in terms of the assumptions we have made. When P_h equals 1.0 moles C m^{-2} yr^{-1} less than 10% of the phosphate transported into the high-latitude box is removed by organisms.

In Figure 5 we illustrate how the P_{CO2} of the atmosphere responses to $f_{\ell d}$, the direct, bidirectional exchange between the low-latitude surface box and the deep sea. In this series of figures, $f_{\ell d}$ increases from 4 to 12 Sv by increments of 4 Sv. The parameter $f_{\ell h}$, bidirectional exchange between the low- and high-latitude surface boxes, is held fixed at 10 Sv; $f_{\ell h}$ is not an easy quantity to estimate for the real ocean, although it is surely not zero, as we assumed for the simple case above. The 10-Sv figure is a guess; it represents an exchange of about one part in 40 per year for the high-latitude box. Because exchange between the low- and high-latitude surface boxes provides an alternate pathway for deep-sea nutrients to reach the low-latitude surface box, lower amounts of upwelling (T) are necessary to account for the observed deep-sea AOU.

The atmospheric P_{CO2} is particularly sensitive to direct exchange between the deep sea and low-latitude surface water. As $f_{\ell d}$ increases from 0 in Figure 4a through 12 Sv in Figures 5a-5c, the atmospheric P_{CO2} increases from 269 to 297 ppm at the intersection of the $\Delta^{14}C$ isolines. The P_{CO2} isolines no longer respond only to T in the f_{hd} versus T parameter space, but instead swing over to respond primarily to f_{hd}, particularly in the lower range of T.

The $\Delta^{14}C$ isolines also respond to $f_{\ell d}$. Because direct mixing between low-latitude surface water and the deep sea increases contact between the deep ocean and atmosphere, an increase in $f_{\ell d}$ must be offset by a drop in f_{hd} or T. Hence, the $\Delta^{14}C_{atm}$ isolines tend to shift downward and to the left in the f_{hd} versus T parameter space. The isolines of $\Delta^{14}C_h$, on the other hand, are not affected by $f_{\ell d}$. Therefore, only T decreases in the model solution as direct exchange between the deep sea and low-latitude surface water increases. When $f_{\ell d}$ is equal to 12 Sv, only 3 Sv of T are

required to meet the ^{14}C constraints. The particle flux from low-latitude surface water increases with $f_{\ell d}$ as more phosphate is delivered to low-latitude surface water. Less high-latitude particle flux is needed to bring AOU_d up to 154 μmol/kg, and we see that the shaded area of the diagrams (P_h less than zero) expands, especially at low values of T.

The rise in atmospheric P_{CO2} in response to direct exchange between the deep sea and low-latitude surface water reveals an important point about how the model works. We see from equation (12) that when T is small, $PO4_h$ increases as $(f_{hd}+f_{\ell d})/f_{hd}$ increases. The increase in $PO4_h$ is mirrored by an increase in high-latitude ΣCO_2 (recall the simplified equation (9)). Less nutrient-depleted water is flushed through the high-latitude box as $f_{\ell d}$ substitutes for T in the ^{14}C balance. Therefore, we might say that the CO_2 content of the atmosphere rises in response to $f_{\ell d}$ because high-latitude surface water becomes more like deep water. We will see in the model simulation for the ice age ocean below that the atmospheric P_{CO2} was lower during the ice age because high-latitude surface water was less like deep water then is observed at present.

We conclude from Figure 5 that only a minimal amount (<4 Sv) of direct exchange between the deep sea and low-latitude surface water is consistent with the preindustrial atmospheric P_{CO2} of 270 ± 10 ppm. This conclusion is, of course, dependent on the assumption which we made about the oxygen content of newly formed deep water. The size of the AOU_h effect on atmospheric P_{CO2} is about the same as the effect of 12 Sv of direct exchange between the deep sea and low-latitude surface water. We will adopt as an optimal solution for the present ocean a set of parameters in which $f_{\ell d}$ equals a token 1 Sv and $f_{\ell h}$ = 10 Sv. (A minimal amount of direct exchange between low-latitude surface water and the deep sea is important when f_{hd} and T are both small.) For our optimal case, f_{hd} is between 45 and 60 Sv and T is about 19 Sv. P_ℓ equals 0.90 moles C m^{-2} yr^{-1}. The preindustrial $\delta^{13}C$ of the atmosphere is -6.18 per mil, while the $\delta^{13}C$ contents of low- and high-latitude surface water are -2.64 and -1.72 per mil, respectively. We will consider P_h to be limited to a range 0 to 1.0 moles C m^{-2} yr^{-1}, which is consistent with the 45-60 Sv range in f_{hd} noted above and with values of $\Delta^{14}C_h$ between -100 and -110 per mil.

The Ice Age Ocean And Atmosphere

We have adapted the model slightly to perform a simulation of ice age conditions. Given Shackleton et al.'s [1983a, b] observation that the $\delta^{13}C$ of the deep sea became lighter by about 0.5 per mil during the ice age, we calculate that approximately 50 μmol/kg of isotopically light (-26 per mil) carbon must have been added to the deep sea. Because the depth of the lysocline seems to have remained the same between glacial and interglacial periods [Broecker, 1982], we assume that an equal amount of $CaCO_3$ dissolved from the seafloor to hold the pH of the deep sea in balance. These changes increase the alkalinity and ΣCO_2 of the deep sea by about 100 μeq/kg and μmol/kg, respectively. Removal of water from the ocean to form continental ice shrinks the ocean volume by 3% and increases the ocean's salinity, phosphate, alkalinity, and ΣCO_2 contents proportionally. We assume that the surface temperature of the low-latitude box decreases to 20.0°C and that of the high-latitude box to 2.0°. Added together, these changes increase the P_{CO2} of the model by 21 ppm at the position in the f_{hd} versus T parameter space which defines today's ocean.

Because we do not know the AOU of the deep sea during the ice age, we allow AOU_d to become a variable quantity. In order to maintain the same degree of determinacy we fix the particulate carbon flux from high-latitude surface water at 0.5 moles C m^{-2} yr^{-1}. All of the other quantities, including AOU_h, the C to P ratio in organic matter, $f_{\ell d}$, and $f_{\ell h}$, remain at the levels for the present ocean as given above. In Figure 6 we present the model results for the ice age simulation. We retain the same f_{hd} versus T parameter space shown in previous results. The pluses mark the position where the $\Delta^{14}C$ = 0 and the $\Delta^{14}C_h$ = -100 isolines meet in the present-day solution.

In figure 6a we plot contours of atmospheric P_{CO2} and $\Delta^{14}C_{atm}$. Atmospheric P_{CO2} values increase from less than 190 ppm at the bottom of the figure to 400 ppm in the upper left-hand corner. The appearance of Figure 6a is radically different from previous P_{CO2} plots because there are no restrictions on AOU_d. Figure 6b shows contours of the deep-box oxygen content overlying a few of the atmospheric P_{CO2} contours from Figure 6a. Model AOU_d values decrease from nearly 375 μmol/kg in the lower right-hand corner of the figure to less than 50 μmol/kg in the upper left. AOU_d increases with increasing T because particle fluxes from low-latitude surface water increase with T. AOU_d decreases with increasing f_{hd} because the ventilation of the deep sea through high latitudes introduces new oxygen without increasing the flux of organic material to the deep sea. Over most of the parameter domain the atmospheric P_{CO2} contours parallel those of AOU_d. In the lower right-hand section of the figures, where the P_{CO2} and AOU_d deviate from one another, the more limited gas exchange capability of CO_2 causes the P_{CO2} to rise with increasing T.

Because we know that the P_{CO2} of the atmosphere during the ice age lies between 200 and 220 ppm [Neftel et al., 1982], we expect to find a model solution for the ice age between the 200- and 220-ppm P_{CO2} isolines in Figure 6a. To reach this region of parameter space, a substantial reduction in f_{hd} is required. The deep-sea oxygen deficit in this region of parameter space lies between 280 and 325 μmol/kg. Because the oxygen content of the deep sea at full saturation would be about 325 μmol/kg at today's average deep-sea temperature,

we see that the model's ice age prediction lies very close to a condition of full anoxia in the deep sea. Although it is not shown here, the phosphate content of high-latitude surface water parallels the AOU_d isolines. To reach the 200-220 ppm P_{CO2} region in Figure 6a requires a reduction in $PO4_h$ from 1.41 μmol/kg to about 0.6 to 0.7 μmol/kg.

From observations by Shackleton et al. [1983b] and others cited by Broecker [1982], we know that the δ^{13} of planktonic forams did not change appreciably between the ice age and recent times. This is equivalent to saying that the δ^{13} content of the low-latitude surface box did not change. In Figure 6c we have plotted the differences between the $\delta^{13}C$ content of low-latitude surface water as obtained from the ice age simulation, and the preindustrial $\delta^{13}C_\ell$ determined above (+2.64 per mil). We see that the 0 isoline, which shows no difference between the ice age and preindustrial, passes through the 200-220 ppm P_{CO2} field directly below the modern solution and at somewhat smaller values of T. If we choose as a representative ice age solution the intersection of the P_{CO2} = 210 ppm and $\Delta\delta^{13}C_\ell$ = 0 isolines in Figure 6c, the model predicts that f_{hd} was only 10 Sv during the ice age, one fifth of its present value, and T was about 12 Sv, a little more than half its present value. The particle flux from low-latitude surface water was lower along with T at 0.55 moles C m^{-2} yr^{-1} down from 0.9 moles C m^{-2} yr^{-1}. In Figure 6a we predict that the $\Delta^{14}C$ content of the ice age atmosphere was about +100 per mil. More significant, perhaps, is the prediction that the $\Delta^{14}C$ gradient between low-latitude surface water and the deep sea was about 200 per mil compared to about 110 per mil for the modern ocean.

In Figure 6d we have plotted the difference in $\delta^{13}C$ between ice age and preindustrial high-latitude surface water ($\delta^{13}C_h$ preindustrial = +1.72 per mil). The model predicts that the $\delta^{13}C$ of high-latitude surface water was more than 0.5 per mil heavier during the ice age.

Figure 7 summarizes our results for the preindustrial and ice age scenarios. Steady state concentrations of oxygen, phosphate, alkalinity, and ΣCO_2 are given for the three ocean boxes. Isotopic ratios for ^{13}C and ^{14}C are given for the ocean boxes and atmosphere. Water fluxes in Sverdrups are indicated alongside the transport arrows, and particle fluxes in moles C per square meter per year are given next to the wiggly arrows. Asterisks indicate that concentrations or fluxes are fixed values.

Sarmiento and Toggweiler [1984] illustrate an ice age scenario in which f_{hd} is held constant and the high-latitude particle flux is allowed to vary. This scenario predicts a 70-ppm decrease in atmospheric P_{CO2} with an increase in the high-latitude particle flux to 5 moles C m^2/yr^{-1}. The effect of a change in high-latitude particle flux on the model is virtually identical to a change in f_{hd} except that the ventilation time for the deep sea would remain at modern values in the former case. Sarmiento and Toggweiler examine the possibility that atmospheric CO_2 changes might be driven by changes in high-latitude insolation acting to increase or decrease the high-latitude particle flux. According to this scenario, high-latitude insolation and particle fluxes may have been enhanced during periods of greater tilt in the earth's axis, e.g., 10,000-15,000 years ago. This possibility has been analyzed in more detail by Knox and McElroy [1984].

We find it hard to imagine, however, that a 10 or 15% change in insolation could produce a 500% change in the organic particle flux from high-latitude surface water. It seems much more physically reasonable that lower ice age P_{CO2}'s were caused by a change in Antarctic circulation or convection which produced a large reduction in f_{hd}, as will be discussed below. This conclusion is shared by Siegenthaler and Wenk [1984]. The important feature common to both of these lower P_{CO2} scenarios is a large reduction in high-latitude nutrient concentrations. We have also adapted the model to Broecker's [1982] shelf erosion hypothesis by increasing the model's deep-ocean phosphate content and have found an interesting result: the P_{CO2} of the atmosphere does not go down with an increase in deep ocean phosphate unless the particle flux from high-latitude surface water is also increased to pull down the surface nutrient content.

An important consequence of the model's ice age scenario is its illustration of how the deep ocean's oxygen content varies with respect to f_{hd} and T (Figure 6b). It is commonly thought that a sluggish ocean circulation leads to deep-sea anoxia. If "sluggish" refers to smaller amounts of both f_{hd} and T, this conception is completely wrong; when f_{hd} and T vary together, the oxygen content of the deep sea remains the same. The oxygen content of the deep sea declines when either (1) the thermohaline overturning becomes more vigorous and f_{hd} remains the same or (2) exchange between the deep sea and surface in high latitudes decreases and T remains the same. Changes in relative quantities of f_{hd} and T alter the deep ocean's oxygen content.

Discussion: What Is f_{hd}?

The combined quantities of f_{hd} and T which are required to account for today's partitioning of ^{14}C amount to some 70 Sv. Literature estimates [Warren, 1981] of the rates of bottom water formation are substantially less. Most agree that the rate of formation of North Atlantic Deep Water (NADW) is about 10 Sv. Amounts of Antarctic Bottom Water (AABW) sinking from Antarctic continental shelves add up to less than 10 Sv.

One might characterize these types of deep and bottom water as extreme end members on potential temperature versus salinity (T/S) diagrams. They are relatively easy to locate in ocean surveys and command the most attention as a result. However, if these extreme types of deep and bottom

water represent the principal means by which the deep ocean is ventilated, the $^{14}C/^{12}C$ ratio in the modern atmosphere would be substantially higher than we observe. Broecker [1979] has estimated that the time scale over which the deep western Atlantic is ventilated is very short (not much more than 100 years) because there is simply no evidence that much ^{14}C decay has occurred. Ten sverdrups of NADW formation will not do the trick.

As a simplification we might think of the formation of extreme T/S water masses as the thermohaline overturning or 'T' process in this model. As described by Warren [1981]

> The sinking that is known to take place seems not to be merely a concomitant of the overall meridional density gradient, because most of it occurs from sheltered, semi-enclosed regions (Antarctic continental shelf, Norwegian Sea, low-latitude marginal seas) where near surface water is drawn in, contained long enough to become exceptionally dense, and then is forced back to the open ocean, sinking to depth because of its high density.

High-density bottom water displaces existing deep water upward, leading to the upwelling component of the T circulation. Because the formation of dense bottom water is generally a high-latitude process, the surface water which is "drawn in" to semienclosed basins must come from lower latitudes. This is especially well illustrated in the North Atlantic, where warm, salty surface water is found at quite high latitudes and gives up great quantities of heat when it cools. We see this process occurring in the GEOSECS surface water P_{CO2}'s [Broecker et al., 1979] which drop dramatically below atmospheric values in the North Atlantic north of 40°. North Atlantic surface water flows poleward and cools at such a rate that the exchange of CO_2 with the atmosphere cannot reequilibrate the upper layers fast enough. We also see evidence for the thermohaline nature of NADW formation in the fact that the North Atlantic is relatively impoverished in nutrients; it maintains a low nutrient inventory because it imports nutrient-poor surface water and exports deep water.

The process which we call f_{hd} is another matter. We have been alluding to f_{hd} as an Antarctic process because the high-latitude Southern Ocean covers such an immense area, and because the high nutrient content of Antarctic surface water seems to reflect frequent contact with deep water. From a global ocean heat blance Gordon [1975] has estimated that 38 Sv of Antarctic Bottom Water must be forming to account for the ocean's heat loss to the atmosphere. In an earlier paper, Gordon [1971] estimated that an upwelling of 60 Sv of upper Circumpolar Deep Water with a salinity of 34.6 per mil is necessary to balance the input of fresh water to the Antarctic surface. This volume of upwelling is consistent with that theoretically generated by Ekman divergence south of the polar front. Gordon [1981] contrasts conditions in the Arctic and Southern oceans. In the Arctic, large amounts of fresh water input produce a strong, sharp pycnocline. Very low nutrient concentrations are found in the low-salinity upper layer. The Antarctic pycnocline is characterized by low stability. A relatively small fresh water input nearly balances an upward thermal bouyancy flux from warm Circumpolar Deep Water.

Although the mass balances require large-scale overturning in the Antarctic of the right magnitude to comply with our f_{hd} requirement, the actual overturning is not easy to observe. Gordon [1982] reports on observations made during 1977 and 1978 in the Weddell Sea in which an extensive patch of anomalously cold deep water was found between 200 and 2700 m. The patch of cold water was about a half degree colder than water in the same area during the early 1970's. Gordon attributes the cold patch to convective mixing between deep water and wintertime surface water during the Weddell Polynya which persisted from 1974-1976 in the same area. The rate of overturning required to produce this feature is estimated to be as high as 15 Sv during the Polynya years. Gordon [1978] has also observed a narrow (14 km radius) cold core eddy east of the Weddell Sea which extended from 200 to 4000 m. This eddy is also thought to have been a remnant feature of wintertime convection.

If 50 Sv of deep water does in fact upwell to the surface, where does it go? Some small fraction of it sinks as bottom water from the Weddell Shelf. Some part flows equatorward and sinks at the Antarctic Convergence to form intermediate water. The remainder must cool and sink back into the mass of Circumpolar Deep Water. Apart from the few verifiable episodes of open ocean convection and perhaps 10-15 Sv of intermediate water formation, it is not easy to find 50 Sv of water sinking around the Antarctic today. We therefore leave the search for f_{hd} partially unfulfilled.

Evidence for Changes in High-Latitude Convection in Antarctic Sediments

From the distribution of opal in Antarctic sediments Cooke and Hays [1982] have claimed that sea ice extended out from the continent on a year-round basis during the ice age. Winter sea ice coverage 18,000 years ago was probably double the present winter sea ice cover. Cooke and Hays claim that summer sea ice covered slightly more area than present winter ice. Although this latter conclusion has been refuted by more recer. work [Burckle et al., 1982], it is clear that the zone of diatomaceous ooze which characterizes modern Antarctic sediments in the zone of seasonally varying sea ice was displaced hundreds of kilometers to the north 18,000 years ago. In two of the cores studied by Cooke and Hays, sedimentation rates averaged more than 30 cm/1000 years; Cooke and Hays are able to show that the pattern

of sedimentation changed within 200 years at these sites about 14,000 years ago, just before or during the beginning stages of important changes in northern hemisphere ice volume [Ruddiman and McIntyre, 1981]. Oeschger et al. [1984] have dated the rise of atmospheric CO_2 levels at the end of the last ice age at about 14,000 years B.P.

Hays et al. [1976a] and Cooke and Hays [1982] have also shown that the abundance of the radiolarian Cycladophora davisiana in Antaractic sediments shows an abrupt decline in conjunction with the southward displacement of silicious ooze at the close of the last ice age. C. davisiana abundance as a percentage of the total radiolarian fauna drops from 30-40% to less than 5% over a wide expanse of the Southern Ocean. Morely and Hays [1983] have shown that high abundances of C. davisiana in modern sediments are found only in the Sea of Okhotsk. Morely and Hays propose that the Sea of Okhotsk represents a modern analogue of oceanographic conditions that existed in high-latitude regions during the late Pleistocene. The present Sea of Okhotsk is capped by a very low salinity upper layer and strong pycnocline, in stark contrast to Antarctic conditions today [Gordon, 1981].

Following Morely and Hays [1983], we propose that surface water around the Antarctic 18,000 years ago was capped by a stable pycnocline which inhibited deep convection. This surface layer was relatively depleted in nutrients and, as a result, the CO_2 content of the atmosphere was lower. At present, upwelling of warm, Circumpolar Deep Water prevents salinities in Antarctic surface water from falling much below 33.8 per mil and provides a substantial amount of the heat needed to melt back Antarctic sea ice in the spring [Gordon, 1981]. This upwelling is driven by Ekman divergence in the cyclonic gyres between the Antarctic Circumpolar Current and the Antarctic coast. The sedimentary evidence suggests that the circulation in these gyres was radically disrupted during the ice age.

What, then, would stir up the cyclonic gyres and restart deep Antarctic convection 14,000 years ago? Changes in the earth's orbital parameters may have increased the shear in the zonal wind field near Antarctica, increased the local Ekman suction, and forced a general meltback of Antarctic sea ice. Or, a decrease in local precipitation or meltwater runoff from the continent might have reduced the stability of the Antarctic water column. Detailed examination of these possibilities is beyond the scope of this paper. We can, however, suggest an oceanographic factor which may have played an important role. The buoyancy flux which causes the present Antarctic water column to be so close to neutral stability comes from deep water which is about 3°C warmer than winter surface water. The warmth of present-day deep water is due to its component of relatively warm, salty North Atlantic Deep Water. Streeter and Shackleton [1979] and Boyle and Keigwin [1982], among others, have shown that the production of NADW was reduced during periods of maximal ice sheet extent and ice sheet growth. The cessation of NADW formation would tend to stabilize the Antarctic water column and lower atmospheric P_{CO2}. Conversely, the return of NADW formation would tend to reduce stability in the Antarctic water column and open up the possibility of deep convection and CO_2 release from the deep ocean.

Other Evidence

The best evidence in favor of our hypothesis, that a change in high-latitude convection is responsible for the glacial to interglacial changes in the CO_2 content of the atmosphere, is the synchroneity of Antarctic sedimentary changes and the atmospheric P_{CO2} change. What other evidence do we have which might be brought to bear on the predictions of this model? The most obvious change predicted for the ice age ocean is the near anoxia of the deep sea. Broecker's [1982] shelf extraction hypothesis predicts an oxygen depletion for the deep sea of the same magnitude. If the average oxygen content of the deep sea was 50 μmol/kg or less, we should expect to see abundant evidence of anoxic sediments in areas where oxygen minima are present today. Vast areas of the deep Pacific should have been in contact with a greatly intensified oxygen minimum zone.

We can find no evidence of an anoxia of this scale. We can, however, offer several reasons for its apparent absence. First, the most oxygenated water in any ocean will be found near the bottom where most of the ocean's sediments are located. Second, if the duration of the intense anoxia were about 10,000 years, we might expect to see only 10 cm of sediment accumulate during this period of time. When oxygen returns to the deep sea and benthic organisms recolonize formerly anoxic areas, their bioturbation may erase the record by oxidizing the 10 cm of anoxic sediment. Areas most likely to preserve a large-scale anoxic event would therefore be (1) in the Pacific at 1000-3000 m depth and (2) in regions of high sediment accumulation. Areas of high accumulation in the Pacific in this depth range would mainly be on continental slopes. Such areas are the least desirable areas to study from a sedimentological point of view because turbidites and slumping make dating very difficult, if not impossible. Therefore, we conclude that although it is unlikely that a major anoxic event could have gone undetected, there are reasons why this might be so. A systematic search in the deep Pacific for evidence of lower oxygen levels is clearly needed.

The model also predicts that the $\delta^{13}C$ content of high-latitude surface water was higher during glacial time by at least 0.5 per mil and that the phosphate content was lower by about 0.7 μmol/kg. Either of these predictions might be verified by measuring the isotopic content of Antarctic planktonic forams or their Cd to Ca ratios [Boyle and Keigwin, 1982]. A fundamental difficulty is that planktonic foraminifera do not thrive in cold

Antarctic waters and are not abundant in Antarctic sediments south of the polar front. Diatoms are much more successful in the Antarctic, where silica is available in abundance.

A better test might be measurement of Cd to Ca ratios in ice age Antarctic Bottom Water. If ice age surface water was dramatically lower in nutrients, the cadmium content should have been lower also [Boyle and Keigwin, 1982]. Therefore, benthic forams living in areas bathed by Antarctic Bottom Water might record the surface water signal. One problem with this idea is that present-day Weddell Shelf Water entrains surrounding deep water as it sinks to the bottom. This will attenuate whatever surface signal is present.

The model predicts that the $\Delta^{14}C$ content of the ice age atmosphere was about +100 per mil, assuming there has been no change in the ^{14}C production rate. The oldest varved lake sediments, taken from Lake of the Clouds, Minnesota, date back to 10,000 years B.P. and have an age-corrected ^{14}C activity of +90-100 per mil [Stuiver, 1971]. Variations in atmospheric ^{14}C have been commonly attributed to changes in the earth's magnetic dipole field. Radiocarbon measurements, like those of the Lake of the Clouds record, are often held out as evidence of a long-term (8000-9000 year) sinusoidal variation in the magnetic field which has caused the ^{14}C production rate to vary. Keir [1983] has investigated the possibility that higher radiocarbon levels in the atmosphere 10,000 years ago might be evidence for a slowdown in deep sea ventilation in combination with a magnetic field oscillation. Longer, independently dated ^{14}C records are needed before atmospheric ^{14}C changes at the glacial-interglacial boundary can be assessed.

Finally, the model predicts that the gradient in $\Delta^{14}C$ between surface water and deep water doubled from present values. The difference between surface and deep water ^{14}C activity should be independent of uncertainties regarding atmospheric ^{14}C production. A promising new technique was unveiled recently to measure this difference in handpicked planktonic and benthic forams which are subjected to accelerator ^{14}C dating [Andree et al., this volume]. Even with the passage of three ^{14}C half-lives a glacial to interglacial signal of 100 per mil should be detectable.

Conclusions

Overturning of the low-stability Antarctic water column makes surface water over a broad expanse of the Southern Ocean much like average deep water with relatively high nutrient and ΣCO_2 contents. As a result, the modern deep sea is well oxygenated, and the atmospheric P_{CO2} is relatively high. We have proposed that during the ice age this overturning was disrupted, leading to a less oxygenated deep sea and a reduced atmospheric P_{CO2}. This proposal is consistent with sedimentological evidence which suggests that the ice age Southern Ocean was capped with an intense pycnocline and a low-salinity upper layer. An abrupt change in Antarctic sedimentation about 14,000 years ago occurs at about the same time that atmospheric CO_2 levels began to rise. We have demonstrated that a fivefold reduction in the rate at which high-latitude surface water exchanges with the deep sea can produce a 70-ppm lowering of atmospheric P_{CO2} and can reproduce the late Pleistocene-Holocene $\delta^{13}C$ changes recorded in ocean sediments.

The four-box model developed here offers a number of predictions about the ice age ocean and atmosphere which may be verifiable in future work. There are as follows:

1. The average oxygen content of the deep sea was within 50 μmol/kg of zero oxygen.
2. The average phosphate content of newly formed deep water was 0.6-0.7 μmol/kg, or about half that of today's Antarctic surface water.
3. The $\delta^{13}C$ content of high-latitude surface water was more than 0.5 per mil heavier than preindustrial values.
4. The ^{14}C content of the atmosphere was about +100 per mil, assuming there has been no change in the ^{14}C production rate in the upper atmosphere.
5. The $\Delta^{14}C$ difference between warm surface water and average deep water increased by 100 per mil over the present difference of about 110 per mil.

Because the time scales over which these glacial to interglacial changes might occur are the same as those which goven the overturning of the ocean (500-1000 years), the climatic forcing of atmospheric CO_2 probably played a pivotal role in amplifying the orbital forcing which paced the climatic changes [Hays et al., 1976b].

Appendix

One can think of the model as a set of simple linear equations which can be solved by algebraic substitution. The actual solution requires a nested iteration scheme, however, because of the nonlinear equation through which the P_{CO2} values of the two surface boxes are computed [Takahashi et al., 1980].

The model equations are given below in their complete form. In contrast to the equations in the text we include the terms $f_{\ell d}$, $f_{\ell h}$, $PO4_\ell$, and AOU_h. The latter two are assumed to be constants which are given to the model as input parameters. We start below with the equations for P_ℓ, P_h describing the phosphorus particle fluxes and proceed to list a full set of equations for $PO4_h$, $PO4_d$, Alk_h, Alk_d, and Alk_ℓ.

$$P_\ell = PO4_d \cdot (T+f_{\ell d}) + PO4_h \cdot f_{\ell h} - PO4_\ell \cdot (T+f_{\ell d}+f_{\ell h}) \quad (A1)$$

$$P_h = PO4_d \cdot f_{hd} - PO4_h \cdot (T+f_{hd}+f_{\ell h}) + PO4_\ell \cdot (T+f_{\ell h}) \quad (A2)$$

$$r_{O2:P} \cdot (P_\ell+P_h) = AOU_d \cdot (T+f_{hd}+f_{\ell d}) - AOU_h \cdot (T+f_{hd}) \quad (A3)$$

Combining equations (A1), (A2), and (A3) and substituting the conservation expression for $PO4_d$ (see equation (11) in text) we find

$$PO4_h = \left[\frac{T+f_{hd}+f_{\ell d}}{T+f_{hd}} \cdot \left(\frac{PO4_T}{V_d} - \frac{AOU_d}{r_{O2:P}} \right) + \frac{AOU_h}{r_{O2:P}} - PO4_\ell \cdot \left(\frac{f_{\ell d}}{T+f_{hd}} + \frac{T+f_{hd}+f_{\ell d}}{T+f_{hd}} \cdot \frac{V_\ell}{V_d} \right) \right] \cdot \left[1 + \frac{T+f_{hd}+f_{\ell d}}{T+f_{hd}} \cdot \frac{V_h}{V_d} \right]^{-1} \quad (A4)$$

In producing Figures 3, 4, and 5, for the preindustrial ocean we start with equation (A4) because AOU_d is a known quantity. We then derive P_ℓ and P_h as in (A1) and (A2).

For an ice age simulation we do not know the AOU of the deep sea. We assume instead that P_h is the same as that given by the preindustrial solution. The phosphate balance for the high-latitude box is then rewritten as in equation (A5):

$$PO4_h = \left[PO4_T \cdot \frac{f_{hd}}{V_d} - P_h + PO4_\ell \left(T + f_{\ell h} - f_{hd} \cdot \frac{V_\ell}{V_d} \right) \right] \cdot \left[T + f_{\ell h} + f_{hd} \left(1 + \frac{V_h}{V_d} \right) \right]^{-1} \quad (A5)$$

P_ℓ can then be calculated using equation (A1) and AOU_d using (A3).

For alkalinity we have

$$Alk_h = \frac{\frac{Alk_T}{V_d} \cdot A - r_{Alk:P} \cdot \left(\frac{B \cdot P_\ell + P_h}{M} \right)}{1 + A \cdot \frac{V_h}{V_d} - f_{\ell h} \cdot \frac{B}{M}} \quad (A6)$$

where

$$M = T + f_{hd} + f_{\ell h}$$

$$N = T + f_{\ell d} + f_{\ell h}$$

$$A = \frac{1}{M} \left(f_{hd} + B \left(T + f_{\ell d} \right) \right)$$

$$B = \frac{T + f_{\ell h} - f_{hd} \cdot \frac{V_\ell}{V_d}}{N + (T+f_{\ell d}) \cdot \frac{V_\ell}{V_d}}$$

$$Alk_d = \left[Alk_h \cdot (M - (T + f_{\ell h}) \cdot \frac{f_{\ell h}}{N} + r_{Alk:P} \left(\frac{T+f_{\ell h}}{N} \cdot P_\ell + P_h \right) \right] \cdot \left[f_{hd} + \frac{(T+f_{\ell h}) \cdot (T+f_{\ell d})}{N} \right]^{-1} \quad (A7)$$

$$Alk_\ell = \left[Alk_d \cdot (T+f_{\ell d}) + Alk_h \cdot f_{\ell h} - r_{Alk:P} \cdot P_\ell \right] / N \quad (A8)$$

The term Alk_T which appears in equation (A6) represents the total number of equivalents of alkalinity in the ocean see (see Table 2).

Solving the ΣCO_2 equations requires iterating to a stable solution. The procedure consists of a $\Sigma CO2_\ell$ loop nested within a $\Sigma CO2_h$ loop. Each loop involves an iterative convergence in which the P_{CO2} and ΣCO_2 are successively recalculated. After each $\Sigma CO2_h$ (outer) loop is completed, a new $\Sigma CO2_d$ and P_{CO2atm} is determined. When the difference between successive values of $\Sigma CO2_h$ reaches a specified minimum, the procedure stops. The ΣCO_2 equations are given below followed by a detailed outline of the entire procedure.

$$\Sigma CO2_h = \left[(\Sigma CO2_T - P_{CO2atm} \cdot V_a) \frac{A}{V_d} - r_{\Sigma C:P} \cdot \left(\frac{B \cdot P_\ell + P_h}{M} \right) + \frac{g_h \cdot \beta_h}{M} \cdot (P_{CO2atm} - P_{CO2_h}) + g_\ell \cdot \beta_\ell \cdot \frac{B}{M} \cdot (P_{CO2atm} - P_{CO2_\ell}) \right] \cdot \left[1 + A \frac{V_h}{V_d} - B \frac{f_{\ell h}}{M} \right]^{-1} \quad (A9)$$

$$\Sigma CO2_d = \left[\Sigma CO2_h \cdot (M - (T+f_{\ell h}) \cdot \frac{f_{\ell h}}{N} + r_{\Sigma C:P} \cdot \left(\frac{T+f_{\ell h}}{N} \cdot P_\ell + P_h \right) - g_h \cdot \beta_h \cdot (P_{CO2atm} - P_{CO2_h}) - \left(\frac{T+f_{\ell h}}{N} \right) \cdot g_\ell \cdot \beta_\ell \cdot (P_{CO2atm} - P_{CO2_\ell}) \right] \cdot \left[f_{hd} + \frac{(T+f_{\ell h}) \cdot (T+f_{\ell d})}{N} \right] \quad (A10)$$

$$\Sigma CO2_\ell = [\Sigma CO2_d \cdot (T+f_{\ell d}) + \Sigma CO2_h \cdot f_{\ell h} - r_{\Sigma C:P} \cdot P_\ell + g_\ell \cdot \beta_\ell \cdot (P_{CO2atm} - P_{CO2_\ell})] / N \quad (A11)$$

where A, B, M, and N are the same as for alkalinity above and β_ℓ and β_h are the CO_2 solubilities according to Takahashi et al. [1980]. The term $\Sigma CO2_T$ which appears in equation (9) represents the total number of moles of CO_2 in the ocean-atmosphere system (see Table 2). The P_{CO2} of the atmosphere is a simple weighted average of P_{CO2_ℓ} and P_{CO2_h}:

$$P_{CO2atm} = \frac{g_\ell \cdot \beta_\ell \cdot A_\ell \cdot P_{CO2_\ell} + g_h \cdot \beta_h \cdot A_h \cdot P_{CO2_h}}{g_\ell \cdot \beta_\ell \cdot A_\ell + g_h \cdot \beta_h \cdot A_h} \quad (A12)$$

where A_ℓ and A_h are the respective areas of the low- and high-latitude ocean boxes.
A complete outline of the solution procedure follows in schematic form.

For a given set of flux parameters (T, f_{hd}, $f_{\ell d}$, and $f_{\ell h}$)

- -determine $PO4_h$ using equation (A4) or (A5).
- -determine P_ℓ and P_h using $PO4_h$ and (A1) and (A2).
- -determine Alk_h, Alk_d, and Alk_ℓ using equations (6A) - (8A).

Guess initial values for $\Sigma CO2_\ell$ and $\Sigma CO2_h$.

- -determine P_{CO2_ℓ} and P_{CO2_h} using Alk_ℓ, Alk_h, the initial values of $\Sigma CO2_\ell$ and $\Sigma CO2_h$, and the P_{CO2} subroutine of Takahashi et al. [1980].
- -determine P_{CO2atm} using equation (A12).
- -determine an initial value of $\Sigma CO2_d$ using (A10).

Begin iteration

- -calculate P_{CO2_ℓ} using Alk_ℓ and $\Sigma CO2_\ell$.
- -calculate a new value of $\Sigma CO2_\ell$ ("$\Sigma CO2_\ell{}^n$") using $\Sigma CO2_h$ and $\Sigma CO2_d$ and equation (A11).
- -test new $\Sigma CO2_\ell$ against old $\Sigma CO2_\ell$ ("$\Sigma CO2_\ell{}^o$").
  - -if 0.002 μmol/kg > ABS ($\Sigma CO2_\ell{}^o - \Sigma CO2_\ell{}^n$), jump out.
  - -$\Sigma CO2_\ell = \Sigma CO2_\ell{}^o + (\Sigma CO2_\ell{}^n - \Sigma CO2_\ell{}^o)/100$
- -calculate P_{CO2_h} using Alk_h and $\Sigma CO2_h$.
- -calculate a new value of P_{CO2atm} using (A12).
- -calculate a new value of $\Sigma CO2_h$ ("$\Sigma CO2_h{}^n$") using equation (A9).
- -test new $\Sigma CO2_h$ against old $\Sigma CO2_h$ ("$\Sigma CO2_h{}^o$").
  - -if 0.0005 μmol/kg > ABS ($\Sigma CO2_h{}^o - \Sigma CO2_h{}^n$), jump out.
  - -$\Sigma CO2_h = \Sigma CO2h^o + (\Sigma CO2_h{}^n - \Sigma CO2_h{}^o)/5$
- -calculate a new $\Sigma CO2_d$ using $\Sigma CO2_h$ and equation (A10).

For the carbon isotopes the same iterative procedure is followed except that values of P_{CO2atm}, P_{CO2_ℓ}, and P_{CO2h} are carried over from the ordinary ^{12}C solutions. Because the P_{CO2}'s for ^{12}C do not have to be recalculated for each iteration, the convergence is much faster.

The ^{13}C and ^{14}C contents of the ocean and atmosphere are expressed in the model in pseudo-ΣCO_2 (concentration) form following the $^{14}C^*$ notation of Craig [1969]. This means that the fractional isotopic deviation from the isotopic reference (i.e., $1 - \delta^{13}C/1000$ or $1 - \Delta^{14}C/1000$) is simply multiplied by the ΣCO_2 or P_{CO2}. Because the isotopic results are converted back into delta notation at the end of a model run, the isotopic ratio of the reference never enters the calculation.

The biological fractionation factors for ^{13}C and ^{14}C, $^{13}\varepsilon$ and $^{14}\varepsilon$, respectively, only apply to the organic fractions of the particle fluxes. Therefore each appears in an expression, $(1-f_{ca})^i\varepsilon + f_{ca}$, when multiplied by P_ℓ and P_h in the isotopic ΣCO_2 equations. Here f_{ca} is the fraction of the carbon flux which is $CaCO_3$; the isotopic fractionation associated with $CaCO_3$ formation or dissolution is assumed to be negligible. $^{13}\varepsilon$ is equal to 0.977; i.e., the per mil fractionation for $^{13}C/^{12}C$ in organic matter is -23 per mil. $^{14}\varepsilon$ is equal to 0.954.

The atmosphere-ocean partial pressure difference for carbon isotope i is written according to Siegenthaler and Munnich [1981] as follows:

$$^iKF \cdot (^if_{as}(T) \cdot {}^iR_{atm} \cdot P_{CO2atm} - {}^if_{sa}(T) \cdot R^i_s \cdot P_{CO2_s})$$

where the subscript s denotes ocean surface, KF is the kinetic fractionation factor, and $^if_{as}$ and $^if_{sa}$ are the temperature dependent thermodynamic fractionation factors for air to sea and sea to air transfer, respectively. The ^iR terms represent the isotopic ratio of isotope i to isotope 12 in the reservoir in question; in our model formulation the ^iR terms appear as $\Sigma^iCO_2/\Sigma^{12}CO_2$, where the $\Sigma^{12}CO_2$ concentration is carried over from the ^{12}C solutions. Table A1 lists the kinetic and air-sea fractionation factors for the modern and ice age temperatures used in the model.

Decay for radiocarbon is expressed by substituting M' and N' below for M and N in the ΣCO_2 equations:

$$M' = T + f_{hd} + f_{\ell h} + \lambda \cdot V_h \quad (A13)$$

$$N' = T + f_{\ell d} + f_{\ell h} + \lambda \cdot V_\ell \quad (A14)$$

where λ is the decay constant for ^{14}C, 1.2097×10^{-4} yr^{-1}, and V_h and V_ℓ are box volumes. The decay of radiocarbon in all of the model reservoirs must be balanced by the input of new ^{14}C to the atmosphere. To account for the addition of new ^{14}C in the equations, we add the expression $\lambda/M' \cdot \Sigma CO2_T$ to the

TABLE A1. Fractionation Factors for Gas Exchange

	Ocean Temperature	$^{13}f_{as}$	$^{13}f_{sa}$	$^{14}f_{as}$	$^{14}f_{sa}$	$^{13}K_F$	$^{14}K_F$
			Modern				
Low-latitude box	21.5	0.99893	0.99091	0.99786	0.98182	0.9995	0.9990
High-latitude box	2.5	0.99884	0.98860	0.99768	0.97720	0.9995	0.9990
			Ice Age				
Low-latitude box	20.0	0.09893	0.99076	0.99786	0.98152	0.9995	0.9990
High-latitude box	2.0	0.99884	0.98854	0.99768	0.97708	0.9995	0.9990

numerator of equation (A9) for $\Sigma CO2_h$ and add $\lambda \cdot \Sigma^{14}CO2_T$ to the numerator of equation (A12) for P_{CO2atm}. We subtract $\lambda \cdot \Sigma^{14}CO2_T$ from the numerator of equation (A10) for $\Sigma CO2_d$.

Acknowledgments. This work has been supported through the Visiting Scientist Program at the Geophysical Fluid Dynamics Laboratory (NOAA grant 04-7-022-44017) and by ARL/NOAA grant NA83RAC00052 and NSF grant OCE-8110155. We would like to thank Arnold Gordon, Robert Stallard, Mitsuhiro Kawase, and Robert Gardiner-Garden for critically reading the manuscript and Susan Leigh for editorial suggestions. We would like to acknowledge Phil Tunison for drafting the figures and Johann Callan for typing the manuscript and preparing the camera-ready copy. Special thanks are due Sol Hellerman and Marty Jackson for their help in data analysis.

References

Andree, M., et al., Accelerator radiocarbon ages on foramimifera separated from deep-sea sediments, this volume.

Boyle, E.A., and L.D. Keigwin, Deep circulation of the N. Atlantic over the last 200,000 yrs: Geochemical evidence, Science, 218, 748-787, 1982.

Broecker, W.S., A revised estimate of the radiocarbon age of North Atlantic Deep Water, J. Geophys. Res., 84, 3218-3226, 1979.

Broecker, W.S., Ocean chemistry during glacial time, Geochim. Cosmochim. Acta, 46, 1689-1705, 1982.

Broecker, W.S., and T.-H. Peng, Gas exchange rates between air and sea, Tellus, 26, 21-35, 1974.

Broecker, W.S., and T.-H. Peng, Tracers in the Sea, Eldigio Press, Lamont-Doherty Geological Observatory, Palisades, N.Y. 1982.

Broecker, W.S., and T.-H. Peng, and R.E. Engh, Modelling the carbon system, Radiocarbon, 22, 565-598, 1980.

Broecker, W.S., T. Takahashi, H.J. Simpson, and T.-H. Peng, Fate of fossil fuel carbon dioxide and the global carbon budget, Science, 206, 409-418, 1979.

Bryan, K., F.G. Komro, S. Manabe, and M.J. Spelman, Transient climate response to increasing atmospheric carbon dioxide, Science, 215, 56-58, 1982.

Burckle, L.H., D. Robinson, and D. Cooke, Reappraisal of sea ice distribution in Atlantic and Pacific sectors of the Southern Ocean at 18,000 yr BP, Nature, 299, 435-437, 1982.

Cooke, D.W., and J.D. Hays, Estimates of Antarctic Ocean seasonal sea-ice cover during glacial intervals, in Antarctic Geoscience, Int. Union of Geol. Sci., Ser. B, No. 4, edited by C. Craddock, pp. 1017-1025, University of Wisconsin Press, Madison, 1982.

Craig, H., Abyssal carbon and radiocarbon in the Pacific, J. Geophys. Res., 74, 5491-5506, 1969.

Ennever, F.K., and M.B. McElroy, Changes in atmospheric CO_2: Factors regulating the glacial to interglacial transition, this volume.

Gordon, A.L., Oceanography of Antarctic waters, in Antarctic Oceanology I, Antarct. Res. Ser., vol. 15, edited by J.L. Reid, pp. 169-203, AGU, Washington, D.C., 1971.

Gordon, A.L., General ocean circulation, in Numerical Models of Ocean Circulation, pp. 39-53, National Academy of Sciences, Washington, D.C., 1975.

Gordon, A.L., Deep Antarctic convection west of Maud Rise, J. Phys. Oceanogr., 8, 600-612, 1978.

Gordon, A.L., Seasonality of Southern Ocean sea ice, J. Geophys. Res., 86, 4193-4197, 1981.

Gordon, A.L., Weddell Deep Water variability, J. Mar. Res., 40, suppl., 199-217, 1982.

Gordon, A.L., C.T.A. Chen, and W.G. Metcalf, Winter mixed layer entrainment of Weddell Deep Water, J. Geophys. Res., 89, 637-640, 1984.

Hays, J.D., J.A. Lozano, N. Shackleton, and G. Irving, Reconstruction of the Atlantic and western Indian Ocean sectors of the 18,000 B.P. Antarctic Ocean, in Investigation of Late Quaternary Paleoceanography and Paleoclimatology, Mem. 145, edited by R.M. Cline and J.D. Hays, pp. 337-372, Geological Society of America, Boulder, Colo., 1976a.

Hays, J.D., J. Imbrie, and N.J. Shackleton, Variations in the earth's orbit: Pacemaker of

the ice ages, Science, 194, 1121-1132, 1976b.
Honjo, S., Material fluxes and modes of sedimentation in the mesopelagic and bathypelagic zones, J. Mar. Res., 38, 53-97, 1980.
Keeling, C.D., and B. Bolin, The simultaneous use of chemical tracers in oceanic studies, Tellus, 20, 17-54, 1968.
Keir, R.S., Reduction of thermohaline circulation during deglaciation: The effect on atmospheric radiocarbon and CO_2, Earth Planet. Sci. Lett., 64, 445-456, 1983.
Knauer, G.A., J.H. Martin, and K.W. Bruland, Fluxes of particulate carbon, nitrogen, and phosphorus in the upper water column of the northeast Pacific, Deep Sea Res., 26A, 97-108, 1979.
Knox, F., and M. McElroy, Changes in atmospheric CO_2: Influence of marine biota at high latitudes J. Geophys. Res., 89, 4629-4637, 1984.
Kroopnick, P., Correlations between $\delta^{13}C$ and ΣCO_2 in surface waters and atmospheric CO_2, Earth Planet. Sci. Lett., 22, 397-403, 1974.
Levitus, S., Climatological Atlas of the World Ocean, NOAA Prof. Pap. 13, U.S. Government Printing Office, Washington, D.C., 1982.
Li, Y.-H., T. Takahashi, and W.S. Broecker, Degree of saturation of $CaCO_3$ in the oceans, J. Geophys. Res., 74, 5507-5525, 1969.
Manabe, S., and R.J. Stouffer, Sensitivity of a global climate model to an increase of CO_2 concentration in the atmosphere, J. Geophys. Res., 85, 5529-5554, 1980.
Morely, J.J., and J.D. Hays, Oceanographic conditions associated with high abundances of the radiolarian Cycladophora davisiana, Earth Planet. Sci. Lett., 66, 63-72, 1983.
Neftel, A., H. Oeschger, J. Schwander, B. Stauffer, and R. Zumbrunn, Ice core measurements give atmospheric P_{CO2} content during the past 40,000 yrs., Nature, 295, 220-223, 1982.
Oeschger, H., J. Beer, U. Siegenthaler, B. Stauffer, W. Dansgaard, and C.C. Langway, Late glacial climate history from ice cores, in Climate Processes and Climate Sensitivity, Geophys. Monogr. Ser., vol. 29, edited by J.E. Hansen and T. Takahashi, pp. 299-306, AGU, Washington, D.C., 1984.
Peng, T.-H., W.S. Broecker, G.G. Mathieu, and Y.-H. Li, Radon evasion rates in the Atlantic and Pacific oceans as determined during the GEOSECS program, J. Geophys. Res., 84, 7839-7845, 1979.
Redfield, A.C., B.H. Ketchum, and F.A. Richards, The influence of organisms on the composition of sea water, in The Sea, vol. 2, edited by M.N. Hill, pp. 26-77, Wiley-Interscience, New York, 1962.
Ruddimen, W.F., and A. McIntyre, The mode and mechanism of the last deglaciation: Oceanic evidence, Quat. Res., 16, 125-134, 1981.
Sarmiento, J.L., and J.R. Toggweiler, A new model for the role of the oceans in determining atmospheric P_{CO2}, Nature, 308, 621-624, 1984.
Shackleton, N.J., Carbon-13 in Uvigerina: Tropical rainforest history and the equatorial Pacific carbonate dissolution cycles, in The Fate of Fossil Fuel CO_2 in the Oceans, edited by N. Anderson and A. Malahoff, pp. 401-428, Plenum, New York, 1977.
Shackleton, N.J., J. Imbrie, and M.A. Hall, Oxygen and carbon isotope record of east Pacific core V19-130: Implications for the formation of deep water in the late Pleistocene North Atlantic, Earth Planet. Sci. Lett., 65, 233-244, 1983a.
Shackleton, N.J., M.A. Hall, J. Line, and Cang Shuxi, Carbon isotope data in core V19-30 confirm reduced carbon dioxide concentration in the ice age atmosphere, Nature, 306, 319-322, 1983b.
Siegenthaler, U., and T. Wenk, Rapid atmospheric CO_2 variations and ocean circulation, Nature, 308, 624-626, 1984.
Siegenthaler, U., and K.O. Munnich, $^{13}C/^{12}C$ fractionation during CO_2 transfer from air to sea, in Carbon Cycle Modelling, SCOPE 16, edited by B. Bolin, pp. 249-257, John Wiley, New York, 1981.
Stauffer, B., H. Hofer, H. Oeschger, J. Schwander, and U. Siegenthaler, Atmospheric CO_2 concentration during the last glaciation, Proc. Symposium on Ice and Climate Modelling. Annals of Glaciology, in press, 1984.
Streeter, S.S., and N.J. Shackleton, Paleocirculation of the deep North Atlantic: 150,000 year record of benthic foraminifera and oxygen-18, Science, 203, 168-171, 1979.
Stuiver, M., Evidence for the variation of atmospheric ^{14}C content in the late Quaternary, in The Late Cenozoic Glacial Ages, edited by K. Turekian, pp. 57-70, Yale University Press, New Haven, Conn., 1971.
Stuiver, M., H.G. Ostlund, and T.A. McConnaughey, GEOSECS Atlantic and Pacific ^{14}C distribution, in Carbon Cycle Modelling, SCOPE 16, edited by B. Bolin, pp. 201-221, John Wiley, New York, 1981.
Sverdrup, H.U., M.W. Johnson, and R.H. Fleming, The Oceans, Prentice-Hall, Englewood Cliffs, N.J., 1942.
Takahashi, T., W.S. Broecker, A.E. Bainbridge, and R.F. Weiss, Carbonate chemistry of the Atlantic, Pacific, and Indian oceans: The results of the GEOSECS expeditions, 1972-1978, Tech. Rep. 1, CU-1-80, Lamont-Doherty Geol. Obs., Palisades, N.Y. 1980.
Takahashi, T., W.S. Broecker, and S. Langer, Redfield ratio based on chemical data from isopycnal surfaces, J. Geophys. Res., in press, 1984.
Vincent, E., J.S. Killingley, and W.H. Berger, Stable isotopes in benthic foraminifera from Ontong-Java Plateau, box cores ERDC 112 and 123, Palaeogeogr. Palaeoclimatol. Palaeoecol., 33, 221-230, 1981.
Walsh, J.J., Vertical distribution of Antarctic phytoplankton, II, A comparison of phytoplankton standing crops in the Southern Ocean with

that of the Florida Strait, Limnol. Oceanogr., 14, 86-94, 1969.

Warren, B.A., Deep circulation of the world ocean, in Evolution of Physical Oceanography, Scientific Surveys in Honor of Henry Stommel, edited by B. Warren and C. Wunsch, pp. 6-41, MIT Press, Cambridge, Mass., 1981.

Weast, R.C., and M.J. Astle (Eds.), CRC Handbook of Chemistry and Physics, 60th ed., p. F-198, CRC Press, Boca Raton, Fla., 1979.

Weiss, R.F., H.G. Ostlund, and H. Craig, Geochemical studies of the Weddell Sea, Deep Sea Res., 26, 1093-1120, 1979.

Wenk, T., and U. Siegenthaler, The high-latitude ocean as a control of atmospheric CO_2, this volume.